Alma Mater Studiorum · Università di Bologna

Scuola di Scienze
Corso di Laurea Magistrale in Fisica del Sistema Terra

SOLAR RADIATION PENETRATION IN BIOGEOCHEMICAL MODEL OF THE COASTAL OCEAN. NUMERICAL EXPERIMENTS.

Relatore:
Prof. Marco Zavatarelli

Correlatore:
Prof. Xiao Hua Wang

Presentata da:
Anna Maggiorano

Sessione III
Anno Accademico 2015/2016

A Leo,
perchè insieme
siamo fortissimi

ABSTRACT

Questo lavoro si occupa dell'analisi di diversi algoritmi usati per descrivere l'attenuazione della luce in acqua nell'oceano costiero e l'impatto sui processi di produzione primaria usando un modello numerico accoppiato della dinamica biogeochimica marina. Parametrizzazioni nuove e basate sulla letteratura scientifica sono state implementate nel modello numerico unidimensionale BFM-POM. I risultati indicano che una migliore rappresentazione del profilo verticale della luce è ottenuata utilizzando formulazioni basate su un doppio esponenziale, soprattutto quando la parametrizzazione è basata su dati misurati *in situ*. Una migliore rappresentazione dell'ambiente luminoso ha impatto positivo sulla qualità della simulazione della dinamica biogeochimica dell'ambiente marino.

ABSTRACT

This study focuses on the analysis of different algorithms used to describe underwater light attenuation in the coastal ocean and their impact on primary production processes in a numerical coupled model of the marine biogeochemical dynamics. Light parameterizations (novel and literature based) were embedded into the BFM-POM one dimensional modelling system. Results indicated that better representation of the light vertical profiles are obtained with a double exponential formulation, particularly when parameterized on the basis of extensive *in situ* data. Better representation of the light environment impacted positively on the quality of the marine ecosystem biogeochemical dynamics simulation.

See the light as it shines on the sea?
It's blinding
But no one knows
how deep it goes

– How far I'll go (Moana, Disney 2016)

ACKNOWLEDGMENTS

I wish to thank Massimo Celio and the ARPA FVG for providing data,
professor Wang and the UNSW Canberra for the opportunity of working with them,
and professor Zavatarelli for all the help and guidance.

CONTENTS

LIST OF FIGURES

1 INTRODUCTION

Life in the marine environment is based on the inorganic carbon fixation by phytoplankton, via the photosynthetic process, strongly depending on the underwater light availability. In order to perform simulations of the evolution of the marine ecosystem it is important to understand and correctly describe quantitatively how solar radiation is extinguished penetrating the water column.

In this study a biogeochemical numerical model coupled with a one dimensional ocean circulation model (BFM-POM 1D) implemented in the Gulf of Trieste (northern Adriatic Sea) has been used. The model simulates the evolution of the physiological and population processes of the marine environment as constrained by the physical dynamics.
The radiative transfer process numerical representation in governing the primary production biogeochemical process is the focus of this work.

Different parameterizations of underwater light attenuation, obtained from literature and from an original work developed in this thesis has been used in order to evaluate the possible improvements of the algorithm that describes the PAR (Photosynthetic Active Radiation) extinction underwater in the coastal ocean and its effects on the representation of primary production processes.

This dissertation is organised as follows. The basic radiative transfer principles and parameters are described in chapter 2 along with a review of the equations and parameters used in the scientific literature. The photosynthetic process and its relation with the light availability is described in chapter 3.
Chapters 4 and 5 focus on the functioning of the BFM-POM model and its governing equations. The Gulf of Trieste and its main features are presented in chapter 6 along with the description of data collected *in situ* that will be used to evaluate the model calculations and provide an original contribution. In chapter 7 an overview of the data used in order to force the

model will be provided.
Finally, in chapters 8 and 9 the numerical experiments carried out and the results obtained will be illustrated.

2

RADIATIVE TRANSFER IN OCEANIC WATER

DESCRIBING THE RADIATION

In order to describe properly the behaviour of the radiation in oceanic water we need to define some quantities used to physically describe optical radiation. Since we will deal with natural light, which is incoherent, as the phase is not fixed, and composed of photons of different wavelengths, we won't consider a formal description in terms of electric and magnetic fields but we will instead concentrate on measurable quantities following the description of Apel, (1987).

Radiance and irradiance

Quantities that are normally used to indicate the measurable amount of radiation incident on or emitted by a point in space and that could be measured are the radiance and irradiance, defined as follows.

Spectral radiance L_λ could be defined for both emitted or incident radiation as the energy (dQ) per unit time (dt) and unit solid angle ($d\Omega$) incident on a unit area (dA) from the direction ϕ that makes an angle θ with the area in a spectral bandwidth ($d\lambda$):

$$L_\lambda(z,\theta,\phi,t) = \frac{d^4Q}{dt\ dA\ cos\theta\ d\Omega\ d\lambda} \qquad \left[\frac{J}{m^2\ s\ sr\ nm}\right] \quad (2.1)$$

From this quantity we can define the spectral scalar irradiance, which is the power (dW) crossing a unit surface from all directions in a half sphere: $I_\lambda(z) = \frac{dW}{dA\ d\lambda}$, and can be written:

$$I_\lambda(z) = \int_{4\pi} L_\lambda(z,\theta,\phi)d\Omega \qquad \left[\frac{W}{m^2\ nm}\right] \quad (2.2)$$

The scalar irradiance can then be defined for both upwards ($I_{up}(\lambda)$) and downwards ($I_d(\lambda)$) radiation, depending on the direction of the unit area considered.

Both spectral radiance and irradiance can be integrated on the whole spectrum, to obtain the spectrally integrated radiance and irradiance. In particular, by integrating the spectral scalar irradiance over all wavelengths we obtain the total flux of light energy at depth z.

Attenuation coefficient

The amount of light penetrating the water column decays rapidly with depth, due to the interaction of radiation with the water and the different dissolved components. Experimentally, it has been found that irradiance and radiance decay approximately exponentially with increasing depth and different coefficients are then defined to describe this reduction.

The total radiation decay is described by the spectral attenuation coefficient $k_\lambda(z)$, and is due to both absorption and scattering. This coefficient represents the amount of radiation with respect to the total incident radiation, that is extincted as the light goes through the length path dz.
For downwards irradiance the diffuse attenuation coefficient is defined as follow:

$$k_\lambda(z) = -\frac{d}{dz}\ln(I_\lambda) = -\frac{1}{I_\lambda}\frac{dI_\lambda}{dz} \tag{2.3}$$

and the variation in scalar irradiance between depths z and z_1 is then given by:

$$I_\lambda(z) = I_\lambda(z_1)e^{-\int_{z_1}^{z} k_\lambda(z')dz'} \simeq I_\lambda(z_1)e^{-\bar{k}_\lambda(z-z_1)} \tag{2.4}$$

where the approximation is true only if we assume that the attenuation coefficient is constant with depth, which is not always true as concentration of optically active dissolved substances can vary significantly with depth.
Scattering and absorption coefficients are defined similarly and represent the amount of radiation respectively diffused and absorbed by water along a unit depth length.

Since these coefficients depend on the distribution of light sources, especially near the ocean surface, they are called apparent optical properties in contrast with the inherent optical properties, that depend only on the medium and the substances dissolved or suspended in it.

The inherent optical properties are defined by the beam absorption, beam scattering and beam attenuation coefficients, which are given by the fractional loss in power, or the change in monochromatic radiant flux, $d\phi(\lambda)$,of a parallel beam due to absorption, scattering or attenuation by the medium over an infinitesimal increment of path ds. The absorption coefficient (a_λ) is then

$$a_\lambda = -\left(\frac{1}{\phi(\lambda)}\frac{d\phi(\lambda)}{ds}\right)_{abs}, \tag{2.5}$$

the scattering coefficient (b_λ) is given by

$$b_\lambda = -\left(\frac{1}{\phi(\lambda)}\frac{d\phi(\lambda)}{ds}\right)_{scat} \tag{2.6}$$

and the attenuation coefficient (c_λ) is the sum of the two:

$$c_\lambda = a_\lambda + b_\lambda \tag{2.7}$$

The spectral transmittance (t_λ) is defined:

$$t_\lambda = 1 - c_\lambda \tag{2.8}$$

and represents the amount of radiation which is not absorbed or diffused by the medium in the infinitesimal path ds.

PAR (Photosynthetically Active Radiation)

In ocean biological studies we are interested in the total radiant energy available for photosynthesis, usually called PAR (photosynthetically available radiation), which is generally considered as the total photon flux between 400 and 700 nm.

PAR is defined in terms of the flux of quanta, due to the quantized interaction between photons and molecular species in the ocean, and is measured in einsteins per square meter per second (E m^{-2} s^{-1}). It is related to the downwelling irradiance through the relation that gives the energy per quantum $\varepsilon = \hbar\omega = hc/\lambda$, where $h = 6.6255 * 10^{-34}$ J s is the Planck's constant and $c = 2.998 * 10^8$ m/s is the speed of light. The complete relation is then:

$$PAR(z) = \frac{1}{N_0}\int_{400}^{700} I_\lambda(z)\frac{\lambda}{hc}d\lambda \tag{2.9}$$

where $N_0 = 6.022 * 10^{23}\ mol^{-1}$ is the Avogadro number and represents the number of particles contained in a mole of a given substance.

The amount of PAR (I_{PAR}) can also be estimated from total spectrally integrated downwelling irradiance (I_d) if the ratio I_{PAR}/I_d is known or can be predicted. This ratio is usually indicated with ε_{PAR} and varies on daily and seasonal timescales and depends on different parameters such as the location, the solar zenith angle and the wind stress. It is usually considered to be between 0.42 and 0.50, being relatively higher in summer and lower in winter.
In ecosystem modelling the choice of the parameter ε_{PAR} is very important as different PAR fraction values could significantly affect the development of phytoplankton spring blooms as explained by Byun and Cho, (2006).

OPTICAL PROPERTIES OF THE OCEAN

Light penetrating through the water column changes significantly in intensity, spectral composition and angular distribution due to inherent optical properties of oceanic water and its major components: dissolved yellow substances, phytoplankton, particulate organic detritus and and inorganic particles as explained in Kirk, (1994). We will now analyse the roles of these substances in the absorption and diffusion of underwater light, concentrating in particular on the PAR part of the spectrum.

Light absorption

The absorption of pure water is a constant and significant contribution on the absorption of radiation by seawater. Pure water is characterised by an intense absorption band in the infrared part of the spectrum, due to the vibrational absorption of the hydrogen-oxygen bond of the water molecule. The tail of this absorption feature influences the red end of the visible spectrum, where water absorbs significantly, and this results in the typical blue colour of the sea, while in the blue region on the other part of the PAR spectrum pure water is characterised by very little absorption.

There are four components that are especially important for absorption of PAR underwater.
The first one that influences the optical properties of the oceanic water is the so called dissolved yellow substance, which is composed of organic materials carried by rivers into the sea and by materials originating from decomposition of phytoplankton. The absorption due to these materials rises exponentially towards shorter wavelengths and has an important contribute on absorption of blue light underwater.
Secondly, phytoplankton light absorption is due to their characteristic pigments, among which chlorophyll a, and has two maximum, in the blue and red region of the spectrum. This contribution is important for most oceanic water where chlorophyll concentration is high.
Other materials contributing to oceanic water light absorption include all the non-living organic particulate matter. Since the most of it is yellow-brown organic detritus, that derives from the decomposition of phytoplankton, its absorption spectrum is similar to the one of the dissolved yellow colours with shoulders due to some products of the breakdown of photosynthetic pigments.
The last contribute to light absorption underwater is due to inorganic suspended matter, composed of different materials such as silt and clay. Light absorption due to this materials varies markedly depending on the location and particle size, as studied in the work of Baker and Lavelle, (1984).

Light scattering

Pure water has a little contribution to total scattering, but is characterised by different features in the diffusion of light with respect to the dissolved materials. First of all, water scattering of light is equal in the forward or backwards direction and water is then responsible for the major part of the upwelling flux in the ocean, since the bigger particles scattering is concentrated in the forward direction. Furthermore, while scattering of light from different substances doesn't vary much with wavelength, the diffusion of light by water molecules is much more intense in the blue part of the spectrum.

Jerlov classification of water types

The work from Jerlov, (1976) studied how spectral distribution of irradiance shows a maximum at $480 - 500$ nm at the surface and as the light penetrates through the water column, this peak shifts slowly toward 465 nm in clear ocean water (such as east Mediterranean). An asymmetry of the spectral curve develops as the light at violet wavelengths becomes stronger than the light green wavelengths as shown in figure 2.1 (A).
Considering waters characterised by higher turbidity, such as the Caribbean Sea, the asymmetry disappears and the distribution curve becomes symmetrical (figure 2.1 (B)). The decreasing in irradiance transmittance reduces the shortwave part of the spectrum more than the longwave part and shifts the maximum of transmittance toward longer wavelengths because of selective absorption by particles and yellow substance.

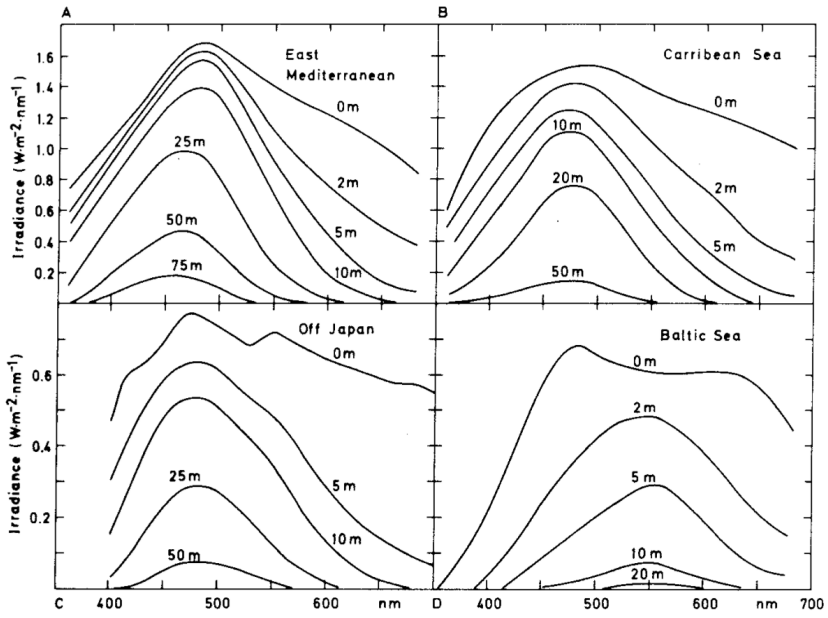

Figure 2.1: Spectral distribution of downward irradiance for high solar elevations in A) Eastern Mediterranean, B) Caribbean Sea, C) Off Japan and D) Baltic Sea. Figure from Jerlov, (1976)

Since optical properties of oceanic water change from place to place due to the different concentrations of suspended particles or dissolved substances in it, Jerlov, (1976) proposed a classification of ocean water types with respect to their optical characteristics in the first 10 meters (which are generally homo-

geneous in the ocean) at high solar altitude. This scheme is now of standard use and divides waters into oceanic (from type I to III, where type I is additionally divided into three subgroups: I, IA and IB) and coastal (from type 1 to 9).
The spirit of the classification is that the irradiance attenuation coefficient for any wavelength can be expressed as a linear function of a reference wavelength, usually chosen at 475 nm.

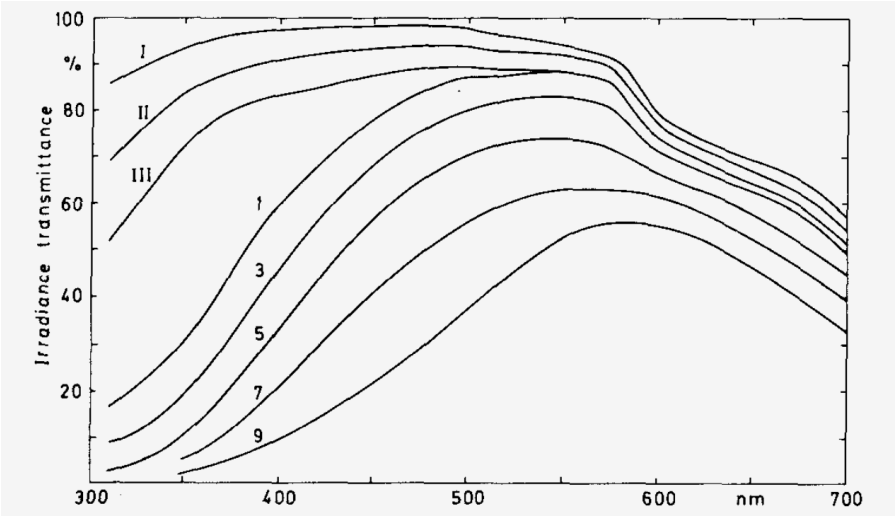

Figure 2.2: Transmittance per meter of downward irradiance in the surface layer for optical water types. Oceanic types I, II, III and coastal types 1, 3, 5, 7, 9 are shown. Figure from Jerlov, (1976)

In particular, as shown in figure 2.2, the difference on the spectral transmittance of different types of oceanic waters is stronger at shorter wavelengths, where in type III waters, the less clear ones, there is a major absorption of particulate material and yellow substance in this part of the spectrum.

SOLAR RADIATION PENETRATION IN THE WATER COLUMN

In order to calculate the vertical profile of downwards irradiance different formulas have been studied in literature. The simplest parameterization is a simple Lambert-Beer's Law equation, with a constant depth-averaged attenuation coefficient k (m^{-1}), using the assumption of optically homogeneous waters:

$$I(z) = I_0 e^{-kz} \tag{2.10}$$

where $I(z)$ is the downwards irradiance at depth z and I_0 is the irradiance at sea surface ($z = 0$). It is widely recognised that this method yields to an overestimation of the penetration of light, especially in the upper few meters.

The observation of selective downwards irradiance absorption at different wavelengths (infrared light is absorbed very rapidly in the first meters of the ocean) led to the development of an improved parameterization by Paulson and Simpson, (1977). Their equation is a double exponential one, with constant coefficients (k_1 and k_2) and an apportioning constant (R) set to fit the observation of downwards irradiance distribution:

$$I(z) = I_0[Re^{-k_1 z} + (1 - R)e^{-k_2 z}] \tag{2.11}$$

In this formulation for the calculation of the attenuation coefficient of the second term only the attenuation of water below 10 meters depth is considered, where many wavelengths have already been extinguished and only the blue-green part of the spectrum is left, and from it is retrieved the attenuation coefficient of the first terms, considering the stronger attenuation of light in the first few meters from the surface. This parameterization is largely used to parameterise the heat flux in the water column.

PAR penetration in the water column

In order to describe how the PAR part of the spectrum penetrates in the water column several changes at the parameterization previously mentioned, which describes the attenuation of the downward irradiance considering the whole spectrum, have been studied in literature.

The simplest PAR parameterization used derives from the Lambert Beer's Law formula 2.10, and is defined inserting a PAR to total irradiance ratio (ε_{PAR}) into the equation:

$$I_{PAR}(z) = I_0 \varepsilon_{PAR} e^{-kz} \tag{2.12}$$

where ε_{PAR} varies between 0.42 and 0.50 and k has a constant value that depends on the type of water considered (Byun and Cho, (2006)).

In order to improve the calculation of how the PAR penetrates in the water column the dependence of k on the substances dissolved in it, such as chlorophyll concentration, yellow substance or detritus, has been studied and in literature k has been written as a function of the concentration of the different substances.

Fasham et al., (1983) studied a parameterization that derives from the Paulson and Simpson's one (equation 2.11):

$$I_{PAR}(z) = I_0 \varepsilon_{PAR} [R e^{-k_1 z} + (1 - R) e^{-k_2 z}] e^{-k_C \int_0^z C(z) dz} \quad (2.13)$$

where ε_{PAR} is the usual PAR apportioning constant and the term $e^{-k_C \int_0^z C(z) dz}$ is a term to accounts for the extinction due to chlorophyll which varies with its concentration integrated over depth dz. R, k_1 and k_2 where retrieve by Fasham et al., (1983) using a similar method to Paulson and Simpson, (1977), but considering data specifically collected in the Celtic Sea.

Another parameterization derived from the double exponential equation was studied by Kara et al., (2005) and by Hamme and Emerson, (2006), and considers for the PAR vertical distribution only the second term in 2.11, which represents the radiation that penetrates more in the water column:

$$I_{PAR}(z) = I_0 (1 - R) e^{-k_2 z} \quad (2.14)$$

This equation is very similar to 2.12, but we have to consider the different origin of ε_{PAR} and $(1 - R)$: ε_{PAR} is the ratio of PAR to total solar radiation just above the sea surface whereas R, as well as k_1 and k_2, was retrieved by Paulson and Simpson, (1977) with a least-square fit of downwards irradiance observation.

From some considerations on the overestimation of the attenuation of radiation by 2.13 and on the underestimation of it by 2.14 Byun et al., (2014) proposed a new parameterization in order to calculate PAR from the total solar downwards irradiance above sea surface:

$$I_{PAR}(z) = I_0 [R' e^{-k_1 z} + (1 - R) e^{-k_2 z}] \quad (2.15)$$

The conceptual idea of this parameterization is to use the second term of the double exponential function 2.11, which accounts for the blue-green part of the spectrum, without the conversion factor for PAR. Consequently, the calculated amount of

PAR $(1 - R)$ should be extracted from the total incoming PAR $(I_0 \varepsilon_{PAR})$ just above the sea surface, in order to calculate the amount of PAR in sea surface waters. From this consideration the value of R' is obtained:

$$I_0 R' = I_0 \varepsilon_{PAR} - (1 - R) I_0 \tag{2.16}$$

and then

$$R' = \varepsilon_{PAR} - (1 - R) = R + \varepsilon_{PAR} - 1 \tag{2.17}$$

The work of this thesis is based on the examination of these PAR attenuation parameterizations and their implementation in a biogeochemical model in order to study how well they approximate the attenuation of the PAR radiation underwater. In chapters 8 and 9 two new parameterizations, based on data collected *in situ*, are proposed and compared to the parameterizations described from the literature.

3

PHYTOPLANKTON PRIMARY PRODUCTION

Phytoplankton is a very important constituent of the marine food chain, thanks to their ability to fix carbon with the photosynthetic process. They account for around 1-2% of the total global biomass, but nonetheless they are responsible for between 30-60% of the global annual carbon fixation on Earth (Sakshaug et al., (1997)).
Carbon fixation depends on several parameters, such as light, temperature, nutrients and chlorophyll-a (chl a) concentration, and in order to calculate carbon fluxes in the sea all this parameter have to be considered.

GENERAL DEFINITIONS

Gross photosynthesis is the rate of electron equivalents that have been photochemically extracted from the oxidation of water. If we don't consider respiratory losses this quantity is equal to the gross oxygen production rate of change.
The gross carbon uptake rate covers all the photosynthetic carbon fixation process, whether or not the carbon becomes part of the organism or is exudated into the environment.
The net photosynthesis corresponds to the temporal evolution of oxygen considering all autotrophic respiratory losses. The "net carbon uptake rate" is the carbon uptake rate following all losses to CO_2 due to the oxidation of organic carbon in the cells in daylight. The net rates in terms of carbon uptake and oxygen evolution should be equal.

Gross primary productivity (P) is the gross carbon uptake rate over 24 hours period. The net primary productivity is the organic carbon synthesised by phytoplankton that is available to the next trophic level and represents the carbon uptake rate following all day-time and night-time respiratory losses.
Dissolved organic carbon (DOC) is produced by the cells and is released into the water and is part of both net photosynthetic rate and net primary productivity.

The growth rate is defined as the net turnover rate for particulate carbon (not including production of DOC) provided that the cells are in steady-state growth and is thus related to net primary productivity. The definition of growth rate includes all the losses of energy and matter from the cells, but not the losses of cells due to external factors such as grazing, sinking and horizontal transport.

The depth at which photosynthesis and respiration losses are equal is called compensation depth. Above this point the net primary production is positive, below is negative.
The euphotic zone is the portion of water column that supports the primary production. The euphotic zone is difficult to measure and is commonly assumed to be the water column down to the depth that corresponds to the 1% of the PAR at the surface.
The critical depth is the depth at which the gross carbon uptake integrated along the water column above over the 24 hours period is equal to the water-column integrated respiratory losses above the same depth. It also depends on other loss factors such as grazing, production of DOC and sinking. The critical depth is always deeper than the compensation depth.

CHL A SPECIFIC ABSORPTION COEFFICIENT OF PHYTOPLANKTON

Chlorophyll-a is the terminal and active photosynthetic pigment in light absorption because even if the energy can be captured by accessory photosynthetic pigments, it has to be transferred to Chl a before it can be used for the photochemical reactions. For this reason, Chl a is generally used as an index ("proxy") of the living and photosynthetically active phytoplankton biomass. The chlorophyll-a concentration is usually measured in mg/m^3.

The Chl a specific absorption coefficient $a^*_\phi(\lambda)$ is used for calculating the contribution of phytoplankton on the total absorption coefficient of seawater and how much radiation is absorbed by phytoplankton in bio-optical models of marine primary production. This coefficient depends on many factors of chemical origin (e.g. pigment composition) and physical origin (e.g. packaging), that often results from physiological acclima-

tion to light condition.
When calculating light that is actually absorbed by phytoplankton the coefficient has to be defined with respect to the spectral composition of the light source:

$$\overline{a^*_\phi} = [I_{PAR}]^{-1} \int_{400nm}^{700nm} a^*_\phi(\lambda) I(\lambda) d\lambda \tag{3.1}$$

In our study, when dealing with the radiation attenuation due to chlorophyll-a we will use a parameterization that depends on the Chla concentration as explained in Fasham et al., (1983), that estimated the contribution of phytoplankton to the light attenuation adding an exponential term as in equation 2.13.

PHOTOSYNTHESIS VERSUS IRRADIANCE CURVES

Photosynthesis (P) versus irradiance[1] (E) curves are a graphical representation of the empirical relationship between solar irradiance and photosynthesis and are used to characterise the photosynthetic response of phytoplankton to changes in light intensity. In a P-E graph (figure 3.1) the irradiance values (on the x axis) are related (on the y axis) with the chlorophyll-a specific gross primary productivity (P^*):

$$P^* = \frac{P}{P_l} \tag{3.2}$$

where P_l is the chlorophyll-a concentration.

Photosynthesis and irradiance have a non linear relation, and P versus E response can be described with three major regions, as shown in figure 3.1.
At the lowest irradiances, photosynthetic rates are linearly proportional to irradiance, as the absorption of photons is slower than the capacity rate of steady-state electron transport from water to CO_2.
As the irradiance increases, photosynthetic rate becomes non-linear and rise to a saturation level, at which the rate of photon absorption greatly exceeds the rate of electron transport from

1 In this section Irradiance is denoted by the symbol E instead of I since this symbol is mostly used in biological oceanography.

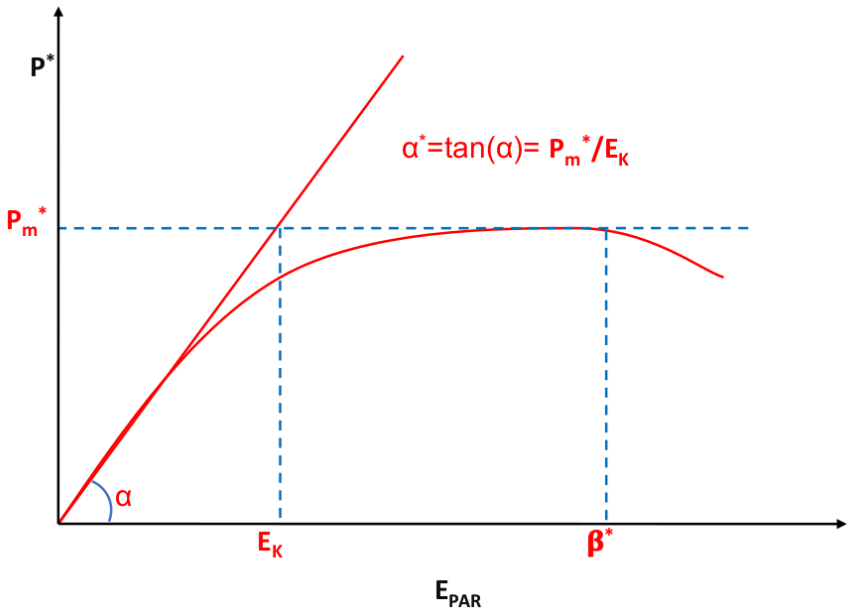

Figure 3.1: A generic P-E graph. Symbols as detailed in the text.

water to CO_2. With further increase in irradiance there is a reduction in the photosynthetic rate with respect to the rate at the saturation level (photoinhibition).

Different parameters define the relation between photosynthesis and irradiance: the initial slope of the P versus E curves α^*, the maximum specific photosynthetic rate P_m^*, the light saturation index (also defined as optimal irradiance) E_k and the photoinhibition parameter β^*.

The parameter α^* characterises the P-E linear relationship at low irradiance, P_m^* indicates the maximum specific photosynthetic rate. E_k is defined by the intercept between α^* and P_m^*. Finally β^* indicates the irradiance value above which photosynthesis starts to be inhibited.The photosynthetic rate in the lower part of the water column is determined by α^* and in the surface layers by P_m^*, while E_k represents the transition zone between the two regimes.

P_m^*, α^* and E_k are the key parameters used by BFM to parameterise photosynthesis and are further discussed in chapter 4. Currently BFM does not consider photoinhibition processes.

4

THE BIOGEOCHEMICAL FLUX MODEL (BFM)

GENERAL INTRODUCTION

The one-dimensional coupled numerical model used is composed of the one-dimensional version of the Princeton Ocean Model (POM) and the Biogeochemical Flux Model (BFM).
The BFM (Vichi et al., (2007)) describes the physiological and population processes of lower trophic levels in the marine environment. Trophic and chemical interaction are described through chemical function families (CFFs) and Living Functional Groups (LFGs), shown schematically in figure 4.1.

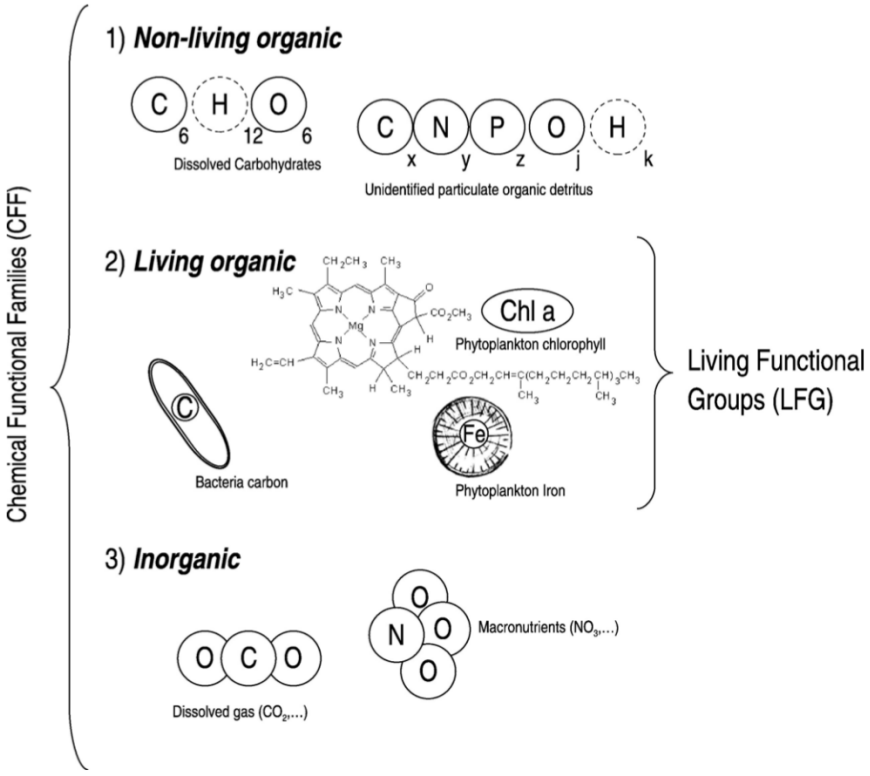

Figure 4.1: Scheme of the various types of Chemical Functional Families (CFFs) expressed in terms of basic biogeochemical elements. Living organic CFFs are the basis for the modelling of Living Functional Groups (LFGs). Figure from Vichi et al., (2007).

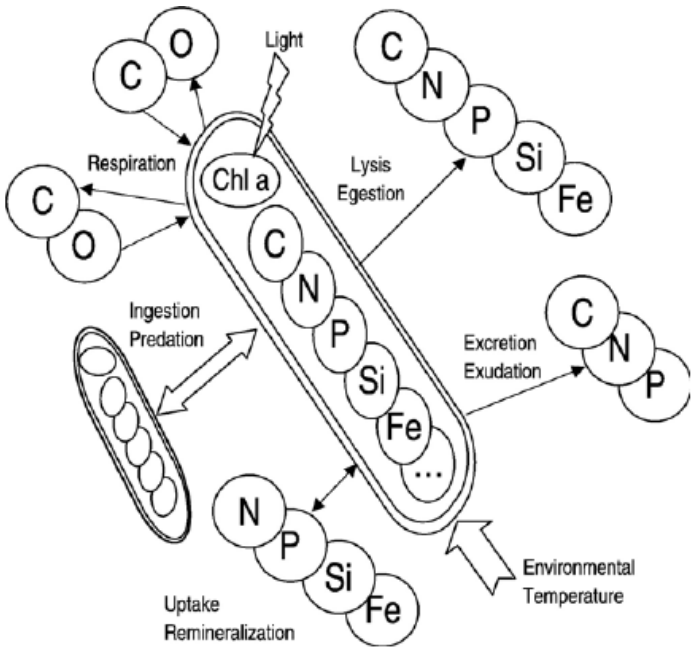

Figure 4.2: Scheme of the standard organism, and the physiological/trophic relationships among the Chemical Function Families and major environmental forcings. Figure from Vichi et al., (2007)

CFFs are defined as the inventory of certain biogeochemical elements contained in more complex living and non-living components of marine biogeochemical cycles or can be sometimes identified as specific compounds such as dissolved inorganic nutrients. CFFs can be described in terms of concentrations and the choice of CFFs as the basic state variables is natural since they are measurable quantities in the limits of laboratory or in situ experiments.
CFFs are divided into three main groups: living organic, non-living organic and inorganic and these groups are measured based on the most important chemical elements: carbon, nitrogen, phosphorus, silicon and oxygen, while hydrogen is not considered a basic constituent in the model.

There are three main Living Functional Groups: producers (phytoplankton), decomposers (bacteria) and consumers (zooplankton) and each of these is defined by internal constituent: carbon, nitrogen, phosphorous, oxygen and silicon (in case of diatoms). The model includes three phytoplankton groups: diatoms, nanophytoplankton and picophytoplankton, and four zooplankton groups: carnivorous mesozooplankton, omnivorous mesozooplankton, microzooplankton and heterophic nanoflag-

ellates. Only one bacteria group is considered.

Members of one LFG are represented by the prototype of a standard organism, shown in figure 4.2. As well as CFFs, also the standard organism is a theoretical construct, which should not be identified with the real organism. The standard organism is thus the model of the LFGs, whose total biomass is composed of living CFFs and interacts with other (living and non-living) CFFs by population processes, such as growth, migration and mortality, and by physiological processes as photosynthesis, ingestion, respiration, excretion and egestion.

The Benthic-Pelagic coupling

Coastal waters and their dynamics are strongly influenced by the shallowness of the sea and by the processes that connect the benthic and the pelagic realms (benthic-pelagic coupling or BPC), whose intensity depends mainly on the water depth. The benthic-pelagic coupling (Mussap and Zavatarelli, (2017)) comprises the two-way exchange of particulate and dissolved matter between the water column and the bottom sediments.

The processes defining the BPC dynamics consist in the sediments -water exchanges, which depend on sinking and resuspension fluxes of the particulate organic matter (POM) and on the oxygen, carbon dioxide and inorganic nutrients diffused at the sediments-water interface.
The biological processes consist on the grazing of the "filter feeders" functional group, which includes the non-moving benthic organisms feeding directly on the pelagic system by filtering the suspended and sinking organic particles. This particle feeding is often also called biodeposition and consists of the extraction of organic matter from the pelagic system and its deposition into the benthic domain in the form of faeces and pseudo faeces. This process add to the benthic-pelagic coupling processes a strongly active component and complements the transfer of organic matter from the water column to the sediments operated by sedimentary fluxes.
The importance of biodeposition process is double: it removes living phytoplankton and contributes to the oxygen and nutrients pool via the bacterial organic matter recycling. Bacterial activity on the deposited organic matter causes the interstitial

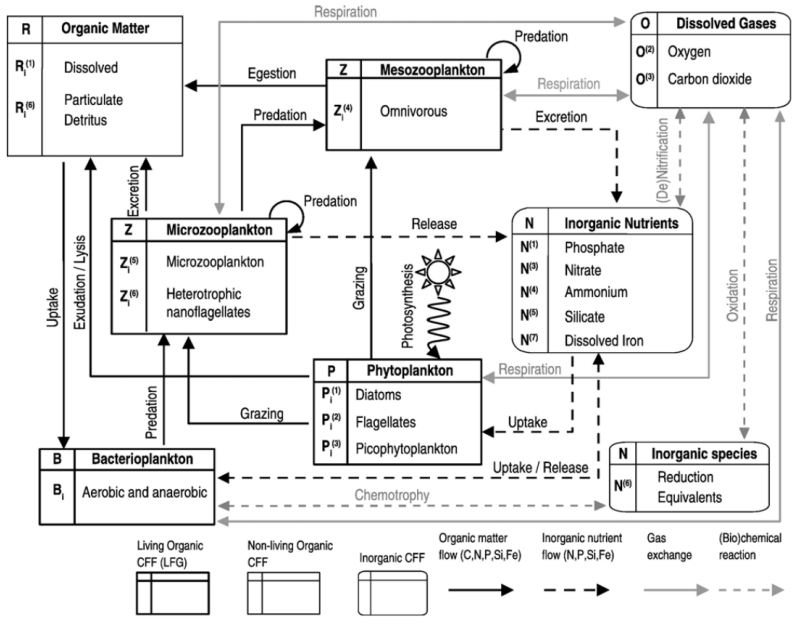

(a)

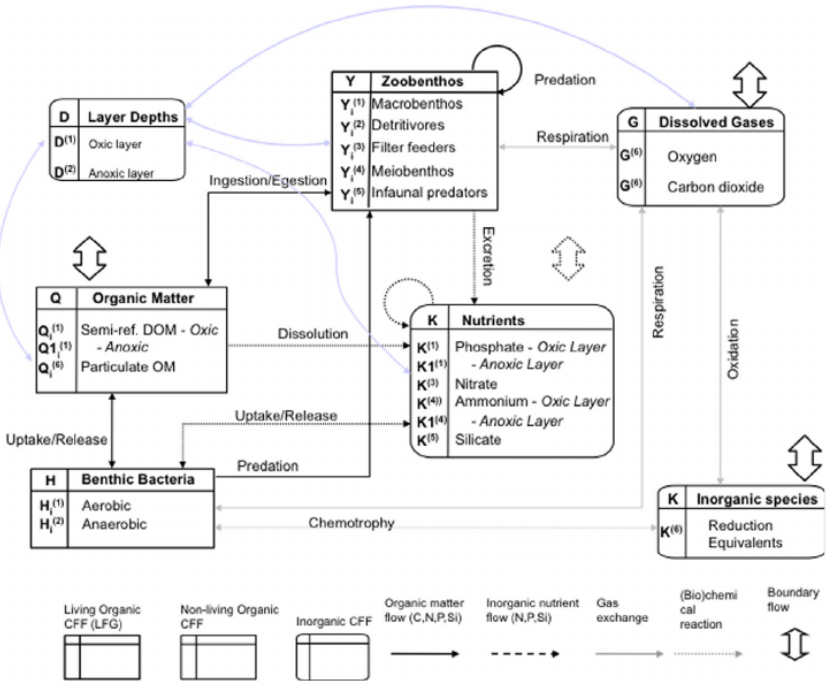

(b)

Figure 4.3: Scheme of the pelagic (a) and benthic (b) interactions and state variables of the biogeochemical model. Living (organic) Chemical Functional Families (CFF) are indicated with bold-line square boxes, non-living organic CFFs with thin-line square boxes and inorganic CFFs with rounded boxes. The fat double-headed arrows indicate fluxes on the benthic-pelagic coupling. Figures from Vichi et al., (2007).

waters to be enriched in inorganic nutrients and carbon dioxide and depleted in oxygen. These differences in concentrations with the overlying water column cause a diffusive exchange back into the water column.

In figure 4.3 are represented two schemes of the pelagic and benthic interactions and state variables of the biogeochemical model.

A scheme of the benthic-pelagic coupling dynamics is shown in figure 4.4.

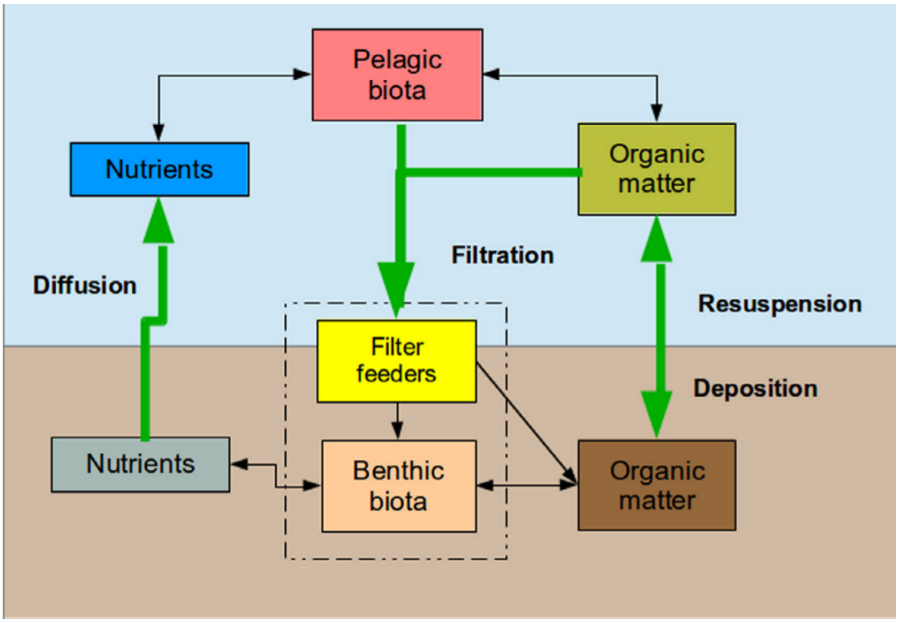

Figure 4.4: Scheme representing the organic and inorganic matter related benthic–pelagic coupling. Green double-headed arrows represent the benthic–pelagic processes of diffusion, filtration, deposition and resuspension. Figure from Mussap and Zavatarelli, (2017).

DYNAMICS OF PRIMARY PRODUCERS

Carbon dynamics

As previously stated, model phytoplankton is composed of several constituents and for each of them dynamical equations are stated. In particular, carbon dynamics is of fundamental importance for the ecosystem and we now want to concentrate on the

processes involved in carbon production.

The processes parameterized in the biological source term are the gross primary production (gpp), respiration (rsp), exudation (exu), cell lysis (lys), nutrient uptake (upt), predation (prd) and biochemical synthesis (syn). The related carbon equation is:

$$\left.\frac{dP_c}{dt}\right|_{bio} = \left.\frac{dP_c}{dt}\right|^{gpp}_{O^{(3)}} - \left.\frac{dP_c}{dt}\right|^{exu}_{R_c^{(2)}} - \left.\frac{dP_c}{dt}\right|^{rsp}_{O^{(3)}} + - \sum_{j=1,6} \left.\frac{dP_c}{dt}\right|^{lys}_{R_c^{(j)}} - \sum_{k=4,5,6} \left.\frac{dP_c}{dt}\right|^{prd}_{Z_c^{(k)}} \tag{4.1}$$

In particular, the first term on the right hand of the equation represents the gross primary productivity and depends strongly on the daylight availability. This term is defined by:

$$\left.\frac{dP_c}{dt}\right|^{gpp}_{O^{(3)}} = f_P^T f_P^E r_P^0 P_c \tag{4.2}$$

In this definition f_P^T is a temperature regulating factor of the form:

$$f_P^T = Q_{10}^{\frac{T-T_{ref}}{T_{ref}}} \tag{4.3}$$

where the Q_{10} coefficient is chosen equal to 2, T is the instantaneous temperature and T_{ref} is a reference temperature (in this study $T_{ref} = 15°C$); r_P^0 is the maximum specific photosynthetic rate and f_P^E is the non-dimensional light regulation factor proposed by Jassby and Platt, (1976), that describes how photosynthesis is controlled by light:

$$f_P^E = 1 - e^{-\frac{I_{PAR}}{E_K}} \tag{4.4}$$

where E_K is the optimal irradiance defined as $E_K = P_m^*/\alpha^*$ (see chapter 3).

Respiration is defined as the sum of basal respiration and activity respiration:

$$\left.\frac{dP_c}{dt}\right|^{rsp}_{O^{(3)}} = \left.\frac{dP_c}{dt}\right|^{brsp}_{O^{(3)}} + \left.\frac{dP_c}{dt}\right|^{arsp}_{O^{(3)}} \tag{4.5}$$

Basal respiration is a function of the carbon biomass P_C, temperature through the regulating factor f_P^T, and the specific constant rate b_P and is then independent of the production rate:

$$\left.\frac{dP_c}{dt}\right|^{brsp}_{O^{(3)}} = b_P f_P^T P_c \tag{4.6}$$

The activity respiration is a constant fraction γ_P of the total gross primary production:

$$\left.\frac{dP_c}{dt}\right|_{O^{(3)}}^{arsp} = \gamma_P \left.\frac{dPc}{dT}\right|_{O^{(3)}}^{gpp} \tag{4.7}$$

The lysis term in equation 4.1 includes all the non-resolved mortality processes that disrupt the cell membrane, such as mechanical causes, virus and yeasts. It is assumed that the lysis rate is partitioned between particulate and dissolved detritus and tends towards the maximum specific rate d_P^0 with a saturation function of the nutrient stress as:

$$\left.\frac{dP_c}{dt}\right|_{R_c^{(6)}}^{lys} = \varepsilon_P^{n,p}\left(\frac{h_P^{p,n}}{f_P^{p,n}+h_P^{p,n}} d_P^0 P_c + \chi^{lys}\right) \tag{4.8}$$

$$\left.\frac{dP_c}{dt}\right|_{R_c^{(1)}}^{lys} = \left(1-\varepsilon_P^{n,p}\right)\left(\frac{h_P^{p,n}}{f_P^{p,n}+h_P^{p,n}} d_P^0 P_c + \chi^{lys}\right) \tag{4.9}$$

where in these equations $\varepsilon_P^{n,p}$ is the percentage of structural parts of the cell going to DOC (Dissolved Organic Carbon) and χ^{lys} is an optional specific lysis rate, included for those phytoplankton populations that are inedible and that acts as an additional mortality term to regulate the population dynamics.

The activity exudation rate is written as:

$$\left.\frac{dP_c}{dt}\right|_{R_c^{(2)}}^{exu} = [\beta_P + (1-\beta_P)(1-f_P^{n,p})]\left.\frac{\partial P_c}{\partial t}\right|_{O^{(3)}}^{gpp} \tag{4.10}$$

and is composed of a constant fraction of carbon uptake (β_P) and a nutrient-related complementary fraction, which is controlled by the internal nutrient ratios according to the Liebig-like regulating factor ($f_P^{n,p}$).

Chlorophyll synthesis

Another important variable describing the planktonic system is given by the chlorophyll (P_l), the pigment used by phytoplankton in order to fix carbon via the photosynthetic process. The chlorophyll equation is:

$$\left.\frac{dP_l}{dt}\right|_{bio} = \left.\frac{dP_l}{dt}\right|^{syn} - \frac{P_l}{P_c}\sum_j \left.\frac{dP_c}{dt}\right|_{Z_c^{(j)}}^{prd} \tag{4.11}$$

where the first term represents the net chlorophyll synthesis, which is mostly derived from Geider et al., (1996), and the second one is given by the losses due to grazing.

In particular, the net chl synthesis is a function of acclimation to light conditions, nutrient availability and turnover rate and is given by:

$$\left.\frac{dP_l}{dt}\right|^{syn} = \rho_{chl}\left(\left.\frac{dP_c}{dt}\right|^{gpp}_{O^{(3)}} - \left.\frac{dP_c}{dt}\right|^{arsp}_{O^{(3)}} - \left.\frac{dP_c}{dt}\right|^{exu}_{R^{(1)}}\right) + - \theta_{chl}\left(\left.\frac{dP_c}{dt}\right|^{lys}_{R^{(1)}} + \left.\frac{dP_c}{dt}\right|^{rsp}_{O^{(3)}}\right) - \max(0, P_l - P_l^{opt})\tau_{chl} \tag{4.12}$$

where θ_{chl} is the instantaneous chlorophyll to carbon ratio (P_l/P_c). In equation 4.12 the first term depends on ρ_{chl}, that regulates the amount of chl in the cell according to a non-dimensional ratio between the realised photosynthetic rate and the maximum potential photosynthesis:

$$\rho_{chl} = \theta^0_{chl}\frac{f^E_P r^0_P P_c}{\alpha^0_{chl} I_{PAR} P_l} \tag{4.13}$$

where θ^0_{chl} is the maximum value of the ratio of chlorophyll over carbon chl/C and α^0_{chl} is the maximum light utilisation coefficient.
The last term in equation 4.12 considers an optimal cell acclimation to light, the theoretical chl concentration that correspond to the optimal value P_l^{opt} is calculated and the system is relaxed to this optimal value in a time scale parameter τ_{chl}.

LIGHT ABSORPTION BY THE WATER COLUMN

Light is fundamental for primary producers and the energy source for photosynthesis is the downwelling amount of the incident solar radiation at the sea surface. In the original formulation of BFM the photosynthetic available radiation (PAR) is parameterized according to the Lambert Beer's formula with depth dependent extinction coefficient, described in Vichi et al., (2007):

$$E_{PAR}(z) = \varepsilon_{PAR} Q_S e^{k_w z + \int_z^0 k_{bio}(z')dz'} \tag{4.14}$$

where ε_{PAR} is the PAR apportioning constant and Q_S is the surface irradiance flux. Light extinction coefficient is composed of two parts: a coefficient that accounts for the background extinction of water k_w and that depends on the Jerlov, (1976) water type considered and an extinction coefficient that depends on the suspended particles k_{bio}.
k_{bio} is written as:

$$k_{bio} = c_{ism} C(ISM) + c_{R^{(6)}} R_c^{(6)} + \sum_{j=1}^{4} c_{P^{(j)}} P_l^{(j)} \tag{4.15}$$

where the extinction due to inorganic suspended matter (ISM), particulate detritus (given by $R_c^{(6)}$) and phytoplankton chlorophyll, for each phytoplankton group, is considered. The c constants are the specific absorption coefficients for each suspended substance, reported in chapter 8.

However, in the following chapters 8 and 9 different parameterizations for the light penetration along the water column studied in literature (as explained in chapter 2) and new parameterizations based on observational data have been implemented and compared.

5

THE COUPLING WITH THE 1D PRINCETON OCEAN MODEL

POM 1D is the one-dimensional version of the three dimensional Princeton Ocean Model (POM), which is a primitive equation ocean circulation model formulated in sigma coordinates (Blumberg and Mellor, (1987)).

POM 1D GOVERNING EQUATIONS

The model adopts the hydrostatic and the Boussinesq approximation. The one-dimensional primitive equations and the equation for the physical tracers are:

$$\frac{\partial u}{\partial t} - fv = \frac{\partial}{\partial z}\left(K_M \frac{\partial u}{\partial z}\right) + F_u \tag{5.1}$$

$$\frac{\partial v}{\partial t} + fu = \frac{\partial}{\partial z}\left(K_M \frac{\partial v}{\partial z}\right) + F_v \tag{5.2}$$

$$\frac{\partial p}{\partial z} = -\rho g \tag{5.3}$$

$$\frac{\partial T}{\partial t} = \frac{\partial}{\partial z}\left(K_H \frac{\partial T}{\partial z}\right) + F_T - \frac{\partial R}{\partial z} \tag{5.4}$$

$$\frac{\partial S}{\partial t} = \frac{\partial}{\partial z}\left(K_H \frac{\partial S}{\partial z}\right) + F_S \tag{5.5}$$

$$\frac{\partial q_2}{\partial t} = \frac{\partial}{\partial z}\left(K_H \frac{\partial q_2}{\partial z}\right) + \frac{2g}{\rho_0} K_H \frac{\partial \widetilde{\rho}}{\partial z} - \frac{2q_2^3}{B_1 l} + F_q \tag{5.6}$$

$$\begin{aligned} \frac{\partial q_2 l}{\partial t} =& \frac{\partial}{\partial z}\left(K_Q \frac{\partial q_2 l}{\partial z}\right) + \frac{l E_1 g}{\rho_0} K_H \frac{\partial \widetilde{\rho}}{\partial z} + \\ & - \frac{q_2^3}{B_1}\left\{1 - \left\{E_2\left[\frac{lH}{\kappa z\,(H+z)}\right]^2\right\}\right\} + F_l \end{aligned} \tag{5.7}$$

Where u, v (m/s) are the mean velocity components; T $(°C)$ and S (psu) are the mean potential temperature and salinity vertical profiles; H (m) is the bottom depth; f is the Coriolis parameter; p (N/m^2) is the pressure; ρ, ρ_0 (kg/m^3) are the instantaneous and reference seawater density respectively; R (Km/s) is the fraction of the solar radiation that penetrates the surface.

Twice the kinetic energy (q_2), twice the kinetic energy times the turbulence length scale ($q_2 l$) and the turbulence vertical diffusivities K_M, K_H and K_Q (m^2/s) are provided by the Mellor and Yamada (1982) turbulence closure scheme. In equations 5.6 and 5.7 the parameters B_1, E_1 and E_2 are the turbulence closure parameters; $\kappa = 0.4$ is the Von Karman constant and

$$\frac{\partial \widetilde{\rho}}{\partial z} = \frac{\partial \rho}{\partial z} - \frac{1}{c_s^2}\left(\frac{\partial p}{\partial z}\right) \tag{5.8}$$

where $c_s = c_s(T, S)$ is the speed of sound.

F_u, F_v, F_q, F_l, F_T, F_S parameterize other processes such as molecular diffusion, internal waves and tidal effects and they are responsible for the dyapicnal transport of nutrients between model layers. These terms are written likewise the turbulent diffusion terms:

$$F_u = \frac{\partial}{\partial z}\left(\chi_M \frac{\partial u}{\partial z}\right) \tag{5.9}$$

$$F_v = \frac{\partial}{\partial z}\left(\chi_M \frac{\partial v}{\partial z}\right) \tag{5.10}$$

$$F_q = \frac{\partial}{\partial z}\left(\chi_M \frac{\partial q_2}{\partial z}\right) \tag{5.11}$$

$$F_l = \frac{\partial}{\partial z}\left(\chi_L \frac{\partial q_2 l}{\partial z}\right) \tag{5.12}$$

$$F_T = \frac{\partial}{\partial z}\left(\chi_T \frac{\partial T}{\partial z}\right) \tag{5.13}$$

$$F_S = \frac{\partial}{\partial z}\left(\chi_S \frac{\partial S}{\partial z}\right) \tag{5.14}$$

where χ_M, χ_L, χ_T and χ_S (m^2/s) are background diffusion terms.

THE VERTICAL COORDINATE SYSTEM

The three dimensional POM adopts a bottom following sigma vertical coordinate system:

$$\sigma_{3D} = \frac{z - \eta}{H + \eta} \tag{5.15}$$

where η is the free surface.

In the 1D version the vertical coordinate system reduces to a simple fractional coordinate system:

$$\sigma = \frac{z}{H} \tag{5.16}$$

with $-1 \leqslant \sigma \leqslant 0$ between ocean bottom and surface respectively.

The computational grid is vertically staggered. The sigma coordinate position of all the variables computed by the modelling system is schematised in figure 5.1.

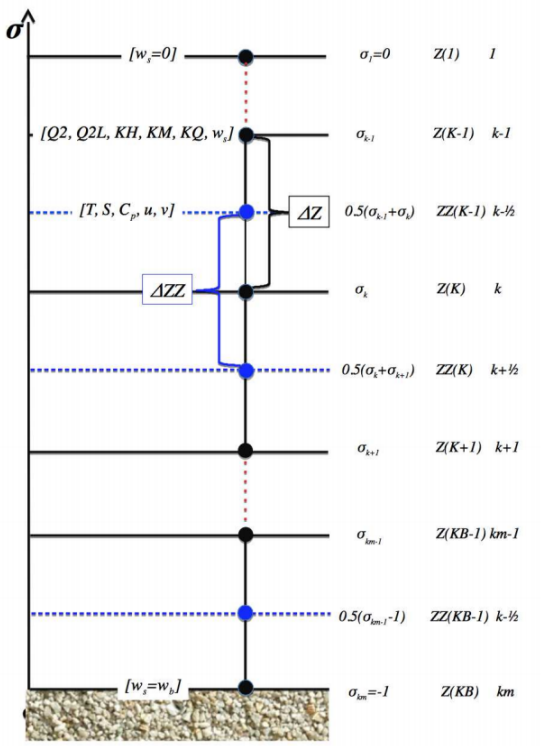

Figure 5.1: The vertically staggered grid of BFM-POM 1D. The picture reports also the computation location of the System state variables. km is the total number of model layers.

The one-dimensional version of the model used is implemented with 30 layers logarithmically distributed near the bottom and surface.

SURFACE AND BOTTOM BOUNDARY CONDITIONS

Boundary conditions at surface

The surface boundary conditions are applied at the depth of surface-most grid point, z_s. For the momentum equation the condition is:

$$\left[(K_M + \chi_M)\frac{\partial(u,v)}{\partial z}\right]_{z=z_s} = \frac{\tau^W_{(x,y)}}{\rho_0} \tag{5.17}$$

For q_2 and q_2l the boundary conditions are:

$$q_{2|_{z=0}} = (B_1)^{\frac{2}{3}}\left[\left(\tau^W_{(x)}\right)^2 + \left(\tau^W_{(y)}\right)^2\right] \tag{5.18}$$

$$q_2 l|_{z=0} = 0 \tag{5.19}$$

$\tau^W_{(x,y)}$ (N/m^2) is the wind stress and the suffix x and y represent the zonal and meridional components. It is an external forcing function and has to be provided to the model.

For the temperature the surface boundary condition is:

$$\left[(K_H + \chi_T)\frac{\partial T}{\partial z}\right]_{z=0} = (\rho_0 C_p)^{-1}(Q_s - Q_b - Q_e - Q_h) \tag{5.20}$$

where C_p is the seawater specific heat, Q_s is the solar radiation flux, Q_b is the net longwave radiation flux, Q_e is the is the latent heat flux and Q_h is the sensible heat flux.
The salinity surface boundary condition is defined by a virtual salinity flux:

$$\left[(K_H + \chi_S)\frac{\partial S}{\partial z}\right]_{z=0} = \alpha[S^*(0,t) - S(0,t)] \tag{5.21}$$

In alternative, boundary conditions at surface for temperature and salinity could be prescribed by a time-varying surface temperature $T^*(0,t)$ and salinity $S^*(0,t)$:

$$[T(z_s,t), S(z_s,t)] = [T^*(0,t), S^*(0,t)] \tag{5.22}$$

Boundary conditions at sea bottom

The bottom boundary condition for the momentum is:

$$\left[(K_M + \chi_M)\frac{\partial(u,v)}{\partial z}\right]_{z=z_b} = \frac{\tau^B_{(x,y)}}{\rho_0} \tag{5.23}$$

where $\tau^B_{(x,y)}$ is the bottom stress, divided into its meridional and zonal components. It depends on the bottom current velocity at the depth of the bottom-most grid point z_B:

$$\frac{\tau^B_{(x,y)}}{\rho_0} = c_z \left\{[u^2 + v^2]^{0.5}(u,v)\right\}_{z=z_B} \tag{5.24}$$

where c_z is a quadratic bottom drag coefficient:

$$c_z = \max\left\{\frac{\kappa^2}{\left[\ln\left(\frac{H-z_B}{Z_0}\right)\right]^2}, c_{z_{min}}\right\} \tag{5.25}$$

with z_0 the bottom roughness length and $c_{z_{min}}$ the minimum possible c_z value.

The bottom boundary conditions for q_2 and q_2l are:

$$q_{2|_{z=z_B}} = (B_1)^{\frac{2}{3}}\left[\left(\tau^B_{(x)}\right)^2 + \left(\tau^B_{(y)}\right)^2\right]^{0.5} \tag{5.26}$$

$$q_2 l|_{z=z_B} = 0 \tag{5.27}$$

For what concerns temperature and salinity bottom boundary condition an adiabatic condition is applied:

$$\left[(K_H + \chi_{T,S})\frac{\partial(T,S)}{\partial z}\right]_{z=-H} = 0 \tag{5.28}$$

DIAGNOSTIC MODE

A modification of the POM 1D model allows for the performance of diagnostic simulations, done by prescribing climatological time dependent temperature and salinity vertical profiles. The vertical profiles of vertical diffusion coefficients are

computed by the model through the (Mellor and Yamada, 1982) second order turbulent closure scheme.

The use of the "diagnostic" mode eliminates possible drifts in temperature and/or salinity due to the use of non zero surface heat and/or salinity surface fluxes or to the lack of a proper parameterization of the lateral advective fluxes, which are by construction, not contained in a one-dimensional model implementation. The use of the diagnostic mode with climatological data, provides a stable (non-drifting) annual cycle of the vertical density structure, which is particularly suitable when using the numerical model to investigate the coupled marine ecosystem dynamics. Clearly, the reliability of the simulations is crucially dependent on the quality of the assembled climatology.

THE COUPLED EQUATION FOR THE BIOGEOCHEMICAL STATE VARIABLES

The temporal rate of change of a generic pelagic non-conservative BFM chemical function family (CFF) or Living Functional Group (LGF) generally indicated as C_p is:

$$\frac{\partial C_p}{\partial t} = \left.\frac{\partial C_p}{\partial t}\right|_{phys} + \left.\frac{\partial C_p}{\partial t}\right|_{bgc} \tag{5.29}$$

where the first term on the right hand side indicates the rate of change dependent on the physical processes and handled by the POM 1D-BFM coupling and the second term indicates the rate of change due to biogeochemical processes, as explained in the previous chapter. The physical rate of change of C_p is resolved by an equation for a non-conservative state variable to which a term of vertical advection accounting for the sinking process has to be added for certain CFFs or LGFs:

$$\left.\frac{\partial C_p}{\partial t}\right|_{phys} = \frac{\partial}{\partial z}\left[(K_H + \chi_b)\frac{\partial C_p}{\partial z}\right] + \frac{\partial (w_s C_p)}{\partial z} \tag{5.30}$$

where χ_b (m/s^2) is the background diffusion coefficient and $w_s(z,t) \leqslant 0$ (m/s) is a sinking velocity.

Boundary conditions

For all the BFM pelagic chemical function families and living functional groups the surface boundary condition is a "zero flux" condition:

$$\left[(K_M + \chi_b)\frac{\partial C_p}{\partial z}\right]_{z=z_s} = 0 \tag{5.31}$$

with the exception of dissolved nutrients (phosphate, nitrate, ammonium and silicate) and dissolved gasses as oxygen and carbon dioxide.

Regarding the inorganic nutrients, considered the coastal implementation of the 1D BFM-POM, it has been defined a surface boundary condition with an imposed surface flux that accounts for the river-borne nutrients input. The condition is defined by relaxing the prognostically computed surface nutrients concentration (N) to a time varying observed surface value (N^*):

$$\left[(K_M + \chi_b)\frac{\partial N}{\partial z}\right]_{z=z_s} = \gamma[N^*(t) - N(z_s, t)] \tag{5.32}$$

where γ is a relaxation velocity.

For what concerns O_2 and CO_2 the surface boundary condition accounts for the sea-atmosphere exchange fluxes $\Phi_{BFM(O_2,CO_2)}$, computed by a specific procedure based on Wanninkhof, (1992):

$$\left[(K_M + \chi_b)\frac{\partial(O_2, CO_2)}{\partial z}\right]_{z=z_s} = \Phi_{BFM(O_2,CO_2)} \tag{5.33}$$

At surface the sinking vertical velocity is zero for all the state variables:

$$w_s(0, t) = 0 \tag{5.34}$$

At the ocean botttom the pelagic dynamics is coupled with the benthic dynamics as explained in 4.1.1.

INFORMATION FLOW AND NUMERICAL INTEGRATION

The information flow occurring between the model components of the BFM-POM 1D system is schematised in 5.2. Red arrows

indicate the external data (forcing functions) that are needed by the model in both the prognostic and diagnostic mode; blue arrows indicate additional data to be provided for the prognostic mode, while the green arrow indicates the prescribed, time, varying temperature and salinity vertical profiles, required by the diagnostic mode.

The numerical integration method and scheme, used to compute the forward in time solution of all the BFM-POM 1D state variables is the same. The sensitivity of the BFM-POM 1D to coupling technique and to integration schemes has been tested by Butenschön et al., (2012), and it was found that the source splitting (SoS) technique is more accurate. POM 1D uses, for the active tracers, a time integration method based on SoS with a leapfrog scheme. The BFM-POM system carries out the final integration of the non-conservative tracers adopting the same coupling technique and numerical scheme. The leapfrog numerical scheme is adopted also for the integration in time of the benthic particulate organic matter.

The numerical solution of all the BFM-POM 1D state variables is carried out in two steps according to the source splitting technique, involving an explicit and an implicit integration. The explicit leapfrog generate an intermediate solution. It might not be needed and, when needed, involves different equation terms in the specific equation.
The characteristics of the (if needed) explicit leapfrog integration are given below by reporting the equation term in discrete form. In the following n is the time index, k the vertical space index (from sea surface to bottom), ΔZ_k and ΔZZ_k the vertical staggered grid spacing.

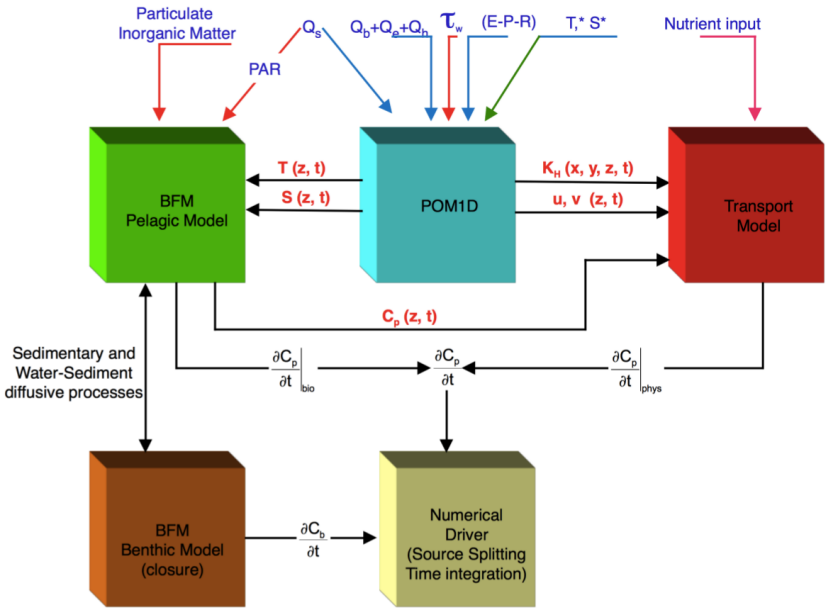

Figure 5.2: Scheme of the information flow between the ocean model and the biogeochemical state variables. The red forcing arrows refer to the use in both the prognostic and diagnostic mode. The blue arrows refer to the use in the prognostic mode only while the green arrows refer to the use in diagnostic mode only. Numerical driver is a generic name for the source splitting solver used to advance in time the coupled solution of the BFM state variables, while the forward in time solution of the physical state variables state variables is embedded in POM 1D.

6

THE GULF OF TRIESTE

GENERAL INTRODUCTION

The BFM-POM 1D model used was implemented in the Gulf of Trieste (Mussap et al., (2016), Mussap and Zavatarelli, (2017)) on the northern-east coast of the Adriatic Sea (shown in figure 6.1).

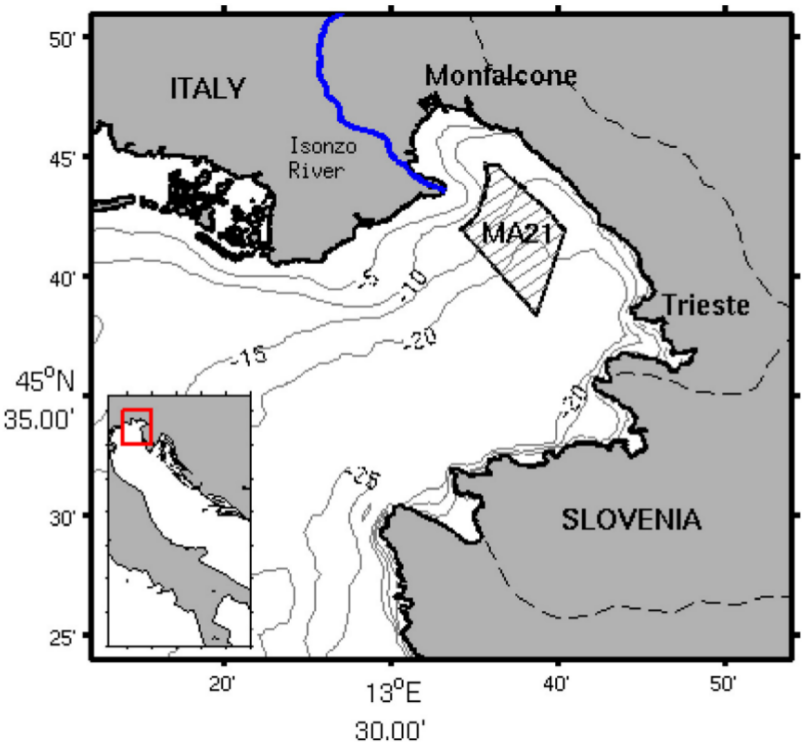

Figure 6.1: Map and bathimetry of the Gulf of Trieste with the location of the area MA21.

The Gulf has an average depth of 20 meters and the whole area is strongly influenced by river runoff, especially along the north-western coast where there is the mouth of the Isonzo River. The implementation area was chosen in the Gulf's macro area identified by the regional environmental agency (ARPA FVG) on the basis of the distance from the coast, geomorphology, hydrological characteristics as water column stability and freshwater inputs. The code of this chosen area is MA21 and is

situated in the centre of the Gulf.

The hydrological features of the Gulf of Trieste show a very large seasonal and inter-annual variability. The circulation is very variable, but the Gulf is generally characterised by a cyclonic circulation driven mainly by the freshwater inputs of the Isonzo ad Po rivers. The tidal currents play a small role in defining the circulation of the Gulf.

The biogeochemical characteristics of the gulf present a significant inter-annual variability due mostly to the variability of the land based nutrient inputs conveyed to the sea mainly by the discharge of the Isonzo River and the anthropogenic pressure. This results in a wide qualitative and quantitative variability in the phytoplankton population structure. The gulf, as most of the Mediterranean Sea, is phosphorous limited and phytoplankton primary production seasonal cycle is characterised by a winter bloom and by high concentration near the seabed during spring and summer.

THE IN SITU OBSERVATION

Monitoring data for the whole area of the Gulf of Trieste were analysed and used to set initial and surface boundary conditions and to validate the performance of the model. This dataset was provided by the regional environmental agency of region Friuli Venezia Giulia (ARPA FVG). The quantities measured by ARPA FVG that we used in our analysis are temperature profiles, salinity profiles, nutrients concentration at surface, PAR profiles, Chlorophyll concentration profiles and dissolved oxygen concentration profiles.

These observation used were the results of a three years (2014-2016) of monthly monitoring program, in different locations of the gulf in the northern Adriatic Sea. The monthly observations were taken the same day between 10 am and 3 pm at different depths with samplings of 0.25 m.

Since we wanted to concentrate on the area situated in the centre of Gulf of Trieste, only the measurements stations in the gulf with depth greater than 10 meters were considered. This approach was adopted in order to ignore the data taken too

close to the coast. The measurement stations considered are shown on the map in figure 6.2.

Figure 6.2: Locations of the measurement stations in the Gulf of Trieste.

INSTRUMENTATION

The *in situ* measurements were taken using the *multiparametric Idronaut mod. 316 Plus* probe shown in figure 6.3.

The basic configuration is equipped for the measurements of:

- Pressure
- Temperature
- Conducibility
- pH
- Dissolved oxygen (misured with a polarographic sensor)

Furthermore the probe is also equipped with the following sensors:

Figure 6.3: *multiparametric Idronaut mod. 316 Plus* probe used for the *in situ* measurements.

- Optical sensor for the measurement of dissolved oxygen through fluorescence
- *Trilux (Chelsea Technologies Group)* for the measurements of the chlorophyll concentration and turbidity
- *LI-COR Underwater Radiation sensor LI-193 Spherical Quantum Sensor* for the measurements of the PAR radiation in the water column
- *Biospherical Instruments' Quantum Scalar Reference Sensor (QSR-2100)* for the measurements of the PAR radiation at the water surface

Chlorophyll-a measurements

In particular, measurement of the chlorophyll-a concentration is based on the observation of "natural fluorescence", the radiance emitted by phytoplankton cells. The *Trilux (Chelsea Technologies Group)* sensor records natural fluorescence in a narrow band centred around 683 nm.

Surface and underwater PAR

There are two radiometers measuring the solar irradiance: one is located at the upper end of the probe and records the underwater irradiance and the second is located on the boat deck and records the solar radiation incident at the sea surface. The two radiometers are shown in figure 6.4.

Both PAR sensors are spherical and therefore measure the solar irradiance. However, the sensor located on the boat deck has a hemispherical field-of-view cutoff plate ensuring uniform directional response over 2π steradians.
The spectral resolution of the sensor correspond to the PAR part of the spectrum (400-700 nm).

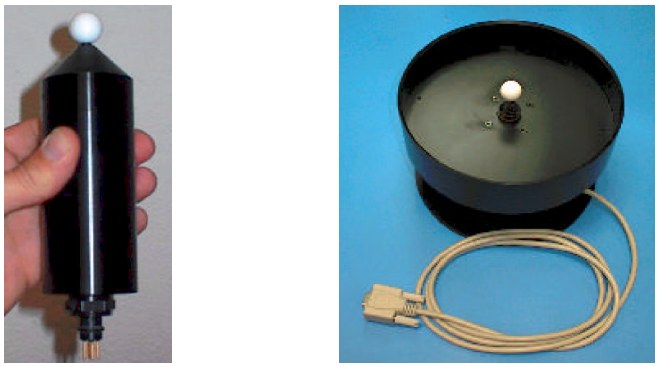

(a) (b)

Figure 6.4: The two radiometers measuring the solar irradiance: a) *LI-COR Underwater Radiation sensor LI-193 Spherical Quantum Sensor* for the measurements of the PAR radiation in the water column, b)*Biospherical Instruments' Quantum Scalar Reference Sensor (QSR-2100)* for the measurements of the PAR radiation at the water surface.

As an example in figure 6.5 is shown an observed underwater vertical profile of PAR radiation, along with the corresponding variability of the surface incident irradiance.

COMPARISON BETWEEN SURFACE AND UNDERWATER PAR

The comparison between the amount of PAR observed underwater with the corresponding surface incident irradiance (as can be seen in figure 6.5) is characterised by a strong decrease of the radiation between the surface measurement and the first underwater measurement at 0.25 m depth. This feature is typical of the data collected *in situ* from the ARPA FVG.

This effect is due in part to the fact that not all the radiation present at the sea surface actually penetrates in the water column as part of it is reflected. The amount of reflected radiation was estimated using a coefficient for the mean albedos at latitude 50N, calculated by Payne, (1972), and then subtracted from the total radiation at sea surface. All following uses of PAR data at sea surface account for this reduction of the amount of radiation.

Even after this correction, the amount of PAR radiation extinguished in the first few centimetres of water is still conspicuous.

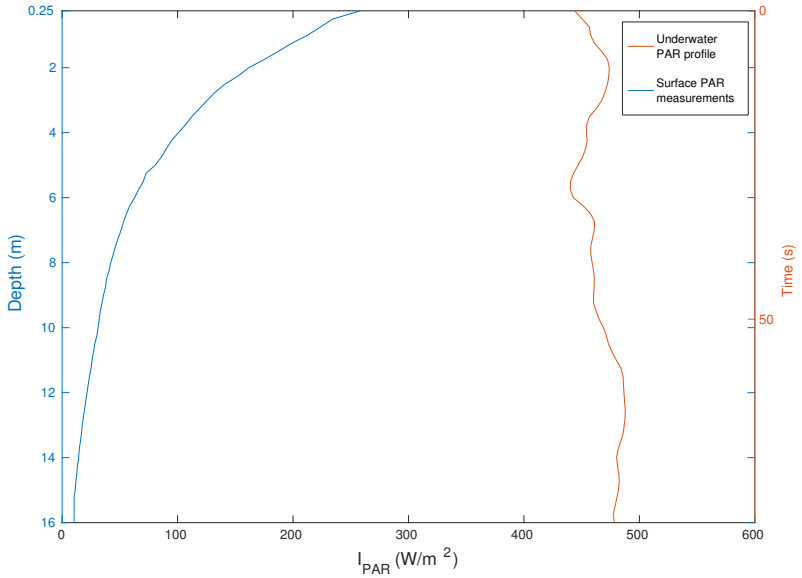

Figure 6.5: Comparison between the observed underwater PAR vertical profile and the corresponding variability of the surface incident PAR irradiance. The data plotted was observed the 13 may 2015 during the sampling taken between 10.26 am and 10.28 am.

This feature has already been reported by Stravisi, (1998), who measured the fraction of PAR irradiance at 0.5 m depth compared to PAR irradiance at the sea surface in the Gulf of Trieste as 0.51 ± 0.14.
Possible causes of this phenomenon could be a higher turbidity than expected for the Gulf of Trieste, or the presence of absorbing materials dissolved in the water.

THE TEMPERATURE AND SALINITY ANNUAL CYCLE

The data of temperature and salinity related to the different locations considered was averaged to obtain a single profile for each month of the year. These climatological (2014-2016) time dependent temperature and salinity vertical profiles obtained were used to perform diagnostic simulations, using the procedure described in the previous chapter.

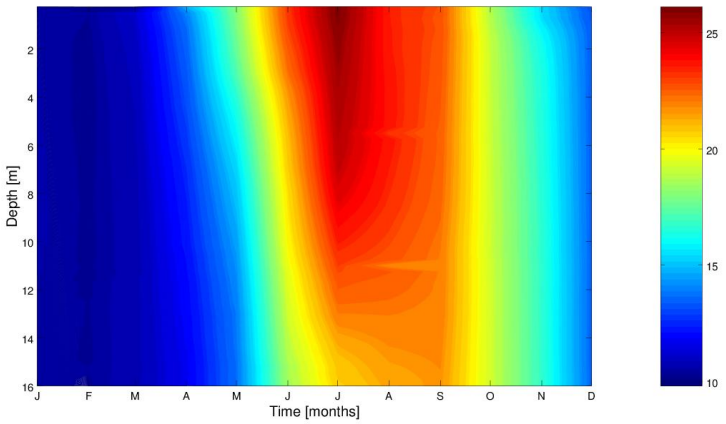

Figure 6.6: Temperature monthly climatological profile calculated from the *in situ* data

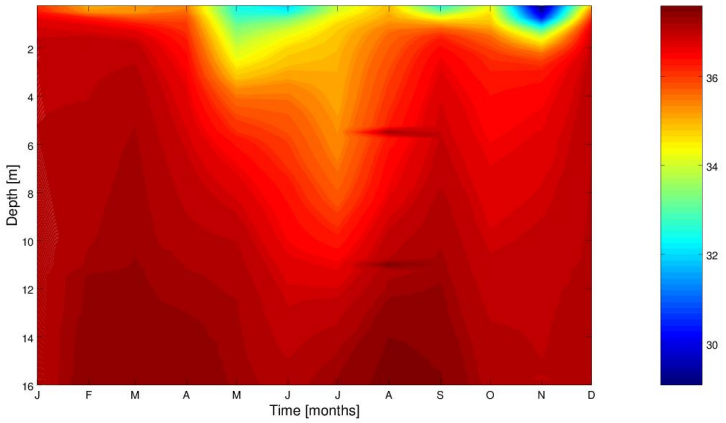

Figure 6.7: Salinity monthly climatological profile calculated from the *in situ* data

Figures 6.6 and 6.7 show the monthly temperature and salinity cycle (respectively). The temperature seasonal cycle is characterised by well-mixed conditions in winter and by vertical thermal stratification in summer. Surface salinity is affected by surface diluting pulses of freshwater mostly due to the Isonzo river discharging in the gulf. Below the surface there are periodical increases in the salinity value due to the ingression of saltier water into the Gulf.

THE SURFACE NUTRIENT CYCLE

The surface nutrients concentration data were used to parameterise the external land based nutrient input according to equation 5.32. The values considered are concentration of nitrate, ammonium, phosphate and silicate (shown in figure 6.8).

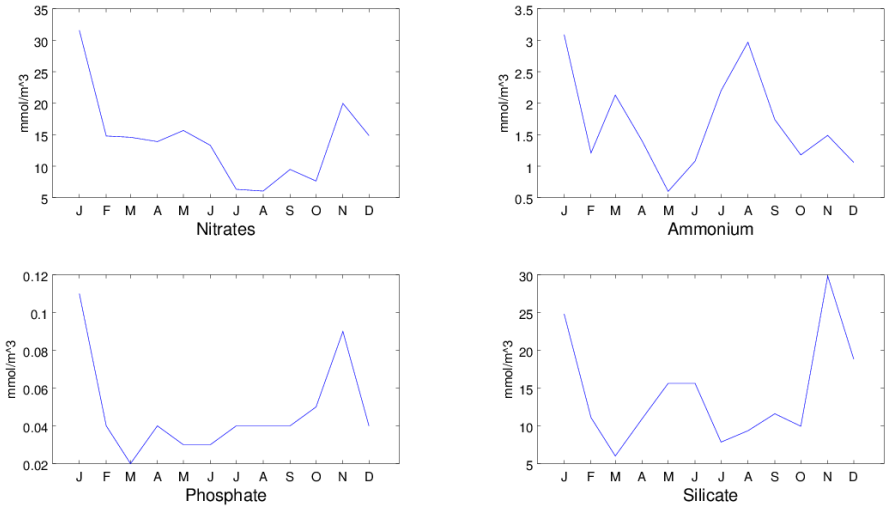

Figure 6.8: Surface monthly varying climatological concentration of nutrients calculated from the *in situ* data

THE OBSERVED ANNUAL CYCLE OF PAR, CHLOROPHYLL AND DISSOLVED OXYGEN

Climatological cycles of PAR (figure 6.9), chlorophyll a (figure 6.10) and dissolved oxygen (figure 6.11) were obtained from the measurements using the procedure described previously for the data of temperature and salinity.

The PAR seasonal cycle shows, as expected, an increase of the amount of radiation incident at surface during summer months, when the value almost doubles with respect to the winter period. The decay of the amount of radiation is almost exponential and the difference in the amount of radiation between summer and winter months decreases as depth increase.
The amount of underwater PAR measured during the month of November is particularly low, this feature is present in the data taken in different years.

From the PAR underwater *in situ* measurements the attenuation coefficients at each depth ($k(z)$) for a simple single exponential attenuation parameterization (described in equation 2.10) were extrapolated.

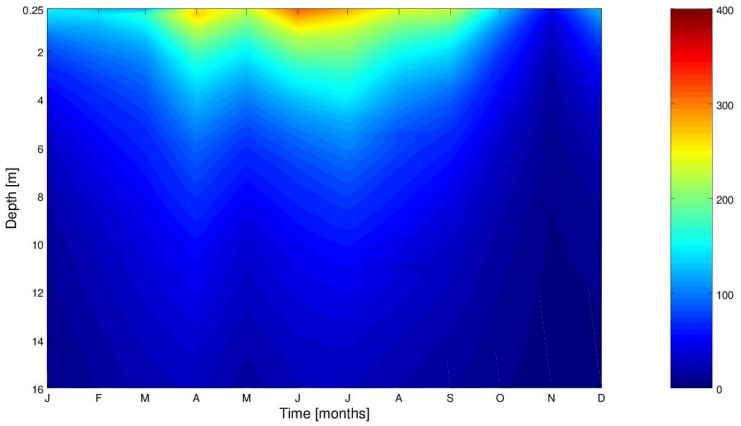

Figure 6.9: Underwater PAR monthly climatological profile calculated from the *in situ* data and measured in (W/m^2)

In figure 6.10, we can see the main feature of the primary production in the Gulf of Trieste, which is characterised by an autumn bloom and by high concentration of chlorophyll near the seabed during spring and summer.

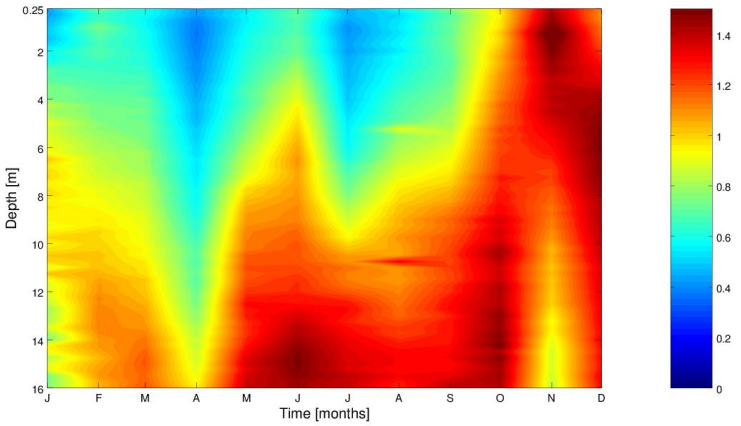

Figure 6.10: Chla a monthly climatological profile calculated from the *in situ* data and measured in (mg/m^3)

The dissolved oxygen seasonal cycle (figure 6.11) is characterised by an uniform and well mixed water column during

winter. In summer, the dissolved oxygen shows stratification in the water column and the low values around the sea bottom are due to the degradation of organic substances.

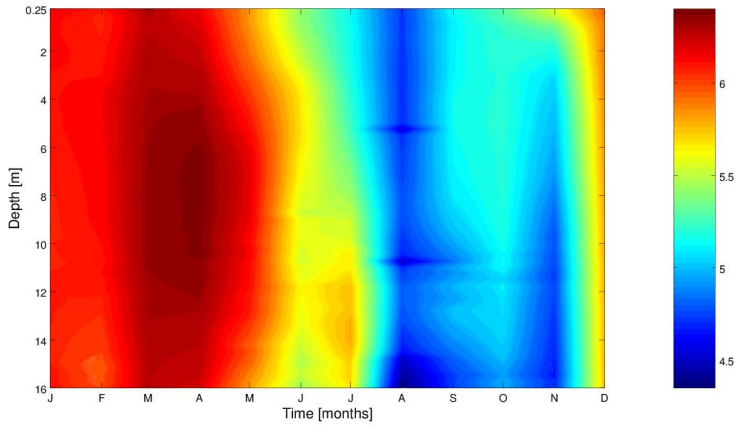

Figure 6.11: Dissolved oxygen concentration monthly climatological profile calculated from the *in situ* data and measured in (ml/l)

7

THE BFM-POM 1D IMPLEMENTATION IN THE GULF OF TRIESTE

The BFM-POM 1D model was implemented in the Gulf of Trieste with 30 σ layers (see equation 5.16) logarithmically distributed near the bottom and surface. The bottom depth is located at 16 meters.
The coupled model combines physics with biology to compute the rate of change of a generic biogeochemical variable (see chapter 5). At each model time step, the hydrodynamic computed by POM provides the BFM with the needed information on the physical environment.

POM was used in a diagnostic mode (as explained in chapter 5), with prescribed monthly varying climatological profiles of temperature and salinity described in chapter 6. The use of the diagnostic mode for the physical components of the modelling system, requires the specification of the surface wind stress as the only surface forcing function.
In order to force the phytoplankton primary production calculated by BFM the net solar radiation incident at the sea surface has to be provided to the model. A monthly varying climatology of nitrate, ammonia, phosphate and silicate is needed to parameterise the land-based surface nutrients input. The data used is described in chapter 6.

We will now describe the specifications of the data used for boundary conditions.

WIND STRESS

The wind stress forcing used was obtained from the 3 hours ECMWF ERA-interim reanalysis (Berrisford et al., 2009) for the years 2014-2016. This time period was chosen in order to be in agreement with the *in situ* measurements of ARPA FVG (see chapter 6). The 3-hours data were averaged in order to obtain a 2014-2016 climatology of the surface wind stress and used as a forcing function for the model. The wind stress module 2014-

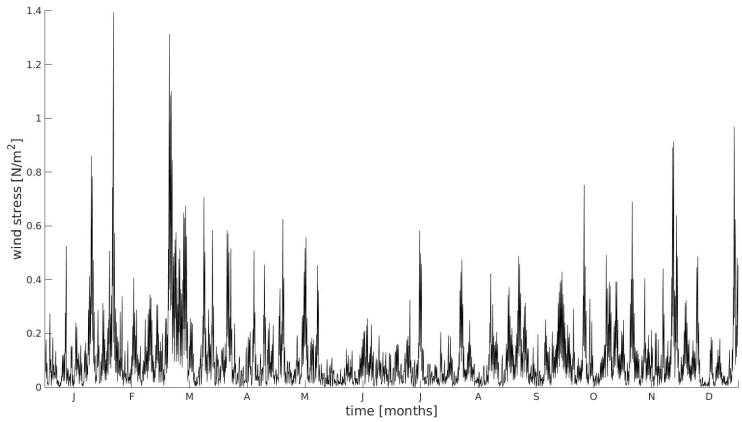

Figure 7.1: Climatological forcing function of wind stress (N/m^2) calculated from the 3 hours ECMWF ERA-interim reanalysis.

2016 climatology time series is shown in figure 7.1.

The wind stress is higher and more variable during winter and autumn, reflecting the influence of the typical strong Bora (northwesterly) and Scirocco (southeasterly) winds, and is weaker and less variable in summer.

SOLAR RADIATION (PAR)

The surface net total solar radiation used to force the primary production was also obtained from the 3 hours ECMWF ERA-interim reanalysis for the years 2014-2016. Using the same procedure illustrated for the wind stress, 3-hours data of different years was averaged in order to obtain a sort of climatology for the net solar radiation incident at the sea surface.

Comparison of ECMWF ERA-interim *data and* in situ *data*

From the net solar radiation at surface data the amount of PAR radiation at surface was obtained applying the PAR apportioning constant $\varepsilon_{PAR} = 0.48$, from Byun and Cho, (2006). The midday monthly mean value of PAR was then considered averaging the radiation values at 12.00, in order to compare with the *in situ* observation from which the estimated albedo fraction (Payne, 1972) has been subtracted as explained in chapter 6. The comparison is shown in figure 7.2.

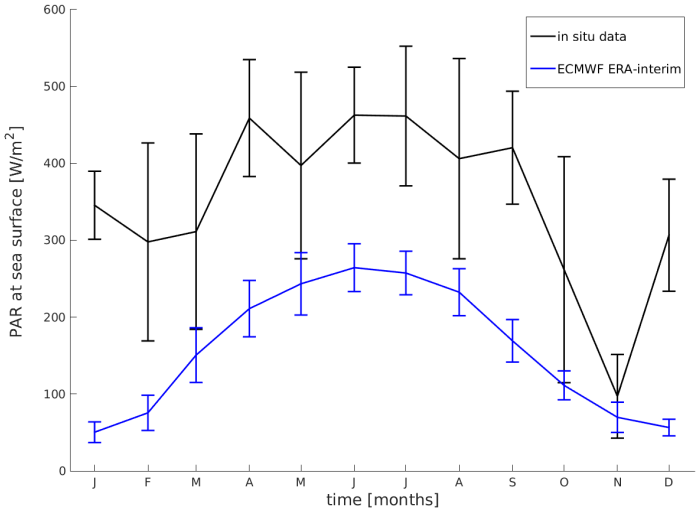

Figure 7.2: Comparison between the PAR irradiance at the sea surface measured *in situ* and the monthly averaged irradiation data provided by ECMWF ERA-interim.

The two data sets differ by a significant amount that varies for each month. In order to have a solar radiation forcing consistent with the *in situ* observations, a correction procedure for the ECMWF ERA-interim solar radiation data has been defined. Such correction was necessary in order to have a forcing surface incident radiation coherent with the observations, so that the underwater irradiance vertical profile generated by the model can be made consistently comparable with the corresponding observed profiles.

The correction had the form:

$$I_{0_{corrected}} = I_0(1 + x) \tag{7.1}$$

where I_0 is the net solar radiation at surface provided by ECMWF ERA-interim and x is the specific adimensional correction factor (shown in table 7.1), calculated for each month from the comparison of the 12.00 data with the PAR data from ARPA FVG. The correction was applied to all the 3 hours step total solar radiation data and the corrected PAR is shown in figure 7.3, along with the comparison with the uncorrected PAR. The figure reports also the observed monthly measurements and it can be noted how the corrected PAR values defined for the model forcing are now matching qualitatively and quantitatively the *in situ* observations.

Month	ECMWF ERA-interim value	ARPA FVG value	Correction factor
Jan	50.38	345.49	5.86
Feb	75.59	297.82	2.94
Mar	150.63	311.22	1.07
Apr	211.04	458.86	1.17
May	243.37	397.21	0.63
Jun	264.36	462.67	0.75
Jul	257.39	461.51	0.79
Aug	232.45	406.10	0.75
Sep	169.22	420.35	1.48
Oct	111.31	261.74	1.35
Nov	69.74	97.09	0.39
Dec	56.47	306.57	4.43

Table 7.1: Monthly average PAR radiation data at surface from ECMWF ERA-interim and *in situ* measurements, with relative calculated correction factors. Values of radiation are in W/m^2.

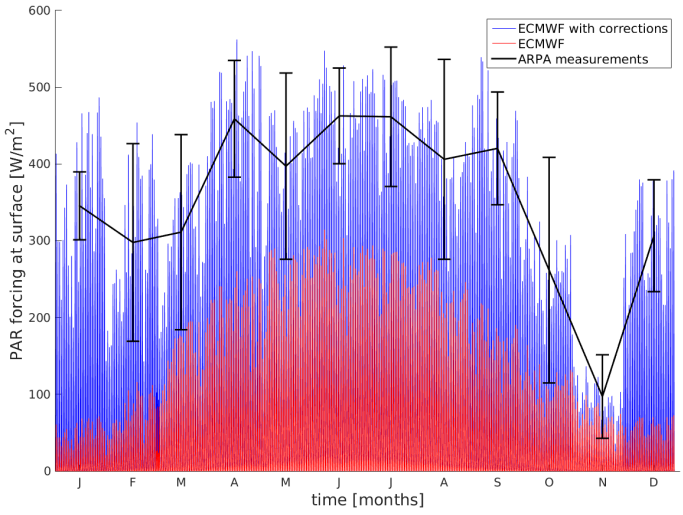

Figure 7.3: Comparison between the PAR irradiance at the sea surface measured *in situ* and the irradiation data provided by ECMWF ERA-interim corrected and uncorrected

The three hours step total solar radiation corrected data was used as model forcing for primary production.

8

NUMERICAL EXPERIMENTS

The main objective of this thesis is to study how different parameterizations of the attenuation underwater of the Photosynthetic Active Radiation (PAR) are able to approximate the solar radiation data measured *in situ* and how a change in the PAR attenuation parameterization influence the biogeochemical model results.
In order to do that a series of numerical experiments with BFM-POM 1D system were performed by implementing different versions and different parameterization of the algorithm defining the PAR vertical penetration along the water column. The procedures were based on the formulations described in chapter 2 with parameters desumed from literature or from the *in situ* observations.

The assessment of the effectiveness of the procedure was then based on the comparison between the observed and simulated underwater PAR and the observed and simulated Chlorophyll-a concentration.

Table 8.1 shows a summary of the different algorithms implemented and the relative parameters used.

In the following a general description of each algorithm used is provided. In all experiments the chosen ε_{PAR} was 0.48.

EXP A

The first parameterization of the PAR attenuation considered is the one that is implemented in BFM by default and described in chapter 4:

$$I_{PAR}(z) = \varepsilon_{PAR} I_0 e^{k_w z + \int_z^0 k_{bio}(z')dz'} \tag{8.1}$$

where I_0 is the total solar radiation flux at the water surface and ε_{PAR} is the PAR to total radiation apportioning constant.

Exp	Attenuation equation	Parameters
exp A	$I_{PAR}(z) = \varepsilon_{PAR} I_0 e^{k_w z + \int_z^0 k_{bio}(z')dz'}$ $k_{bio} = c_{ism} C(ISM) + c_{R^{(6)}} R_c^{(6)} + \sum_{j=1}^{4} c_{P^{(j)}} P_l^{(j)}$	$k_w = 0.12\ (m^{-1})$ $c_{ism} = 0.04 * 10^{-3}\ (m^2/mg)$ $c_{R^{(6)}} = 0.1 * 10^{-3}\ (m^2/mg)$ $c_{P^{(j)}} = 0.03\ (m^2/mg)$
exp B1	$I_{PAR} = \varepsilon_{PAR} I_0 e^{-kz}$	$k = 0.127\ (m^{-1})$
exp B2	$I_{PAR} = \varepsilon_{PAR} I_0 e^{-k(z)z}$	$k(z)$ from ARPA FVG data
exp C	$I(z) = I_0 \varepsilon_{PAR} [R e^{-k_1 z} + (1-R) e^{-k_2 z}] e^{-k_C \int_0^z C(z)dz}$	R=0.51 $k_1 = 0.29\ (m^{-1})$ $k_2 = 0.14\ (m^{-1})$ $k_c = 0.026\ (m^2/mg(Chl))$
exp D1	$I(z) = I_0 [R' e^{-k_1 z} + (1-R) e^{-k_2 z}]$	R=0.78 $k_1 = 0.714\ (m^{-1})$ $k_2 = 0.127\ (m^{-1})$
exp D2	$I(z) = I_0 [R' e^{-k_1 z} + (1-R) e^{-k_2 z}]$	R=0.78 $k_1 = 6.856\ (m^{-1})$ $k_2 = 0.204\ (m^{-1})$
exp E	$I(z) = I_0 [R' e^{-k_1 z} + (1-R) e^{-k_2 z}] e^{-k_C \int_0^z C(z)dz}$	R=0.78 $k_1 = 0.714\ (m^{-1})$ $k_2 = 0.127\ (m^{-1})$ $k_c = 0.026\ (m^2/mg(Chl))$
exp F	$I(z) = I_0 [R' e^{-k_1 z} + (1-R) e^{-k_2 z}] e^{-k_c z}$	R=0.762 $k_1 = 6.447\ (m^{-1})$ $k_2 = 0.163\ (m^{-1})$ $k_c = 0.04\ (m^{-1})$

Table 8.1: Summary of the different algorithms implemented and relative parameters.

It is a simple Lambert Beer's equation where the attenuation coefficient is made of two terms: a coefficient that accounts for the background extinction of water k_w and that depends on the Jerlov, (1976) water type considered and an extinction coefficient that depends on the suspended particles k_{bio}:

$$k_{bio} = c_{ism} C(ISM) + c_{R(6)} R_c^{(6)} + \sum_{j=1}^{4} c_{P(j)} P_l^{(j)} \tag{8.2}$$

where extinction due to inorganic suspended matter (ISM), particulate detritus ($R_c^{(6)}$) and phytoplankton chlorophyll for each phytoplankton group ($P_l^{(j)}$) is considered and the c constants are the specific absorption coefficients for each suspended substance.

EXP B

The simpler parameterization for the PAR attenuation underwater is a simple Lambert Beer's equation (see chapter 2):

$$I_{PAR} = \varepsilon_{PAR} I_0 e^{-kz} \tag{8.3}$$

In *exp B1* k (m^{-1}) is a a constant depth-averaged attenuation coefficient, taken from Byun et al., (2014).

In *exp B2* the coefficient of attenuation is not considered constant with depth and the values at each depth are provided by the *in situ* measurements of the ARPA FVG and interpolated on the model depth grid (see chapter 6).

EXP C

From the parameterization proposed by Paulson and Simpson, (1977) for total downwards radiation (2.11) is derived also the PAR parameterization studied by Fasham et al., (1983) (see chapter 2):

$$I(z) = I_0 \varepsilon_{PAR} [R e^{-k_1 z} + (1 - R) e^{-k_2 z}] e^{-k_C \int_0^z P_l(z) dz} \tag{8.4}$$

where the term $e^{-k_C \int_0^z C(z) dz}$ accounts for the extinction due to chlorophyll which varies with its concentration integrated over

depth dz.

The coefficient used in the implementation of this parameterization in the model are taken from Fasham et al., (1983).

EXP D

A more complex parameterization of the PAR attenuation underwater was proposed by Byun et al., (2014) from a modification of the formulation studied by Paulson and Simpson, (1977) for the attenuation of the total solar radiation (equation 2.11):

$$I(z) = I_0[R'e^{-k_1 z} + (1 - R)e^{-k_2 z}] \tag{8.5}$$

where R is an empirical apportioning constant from which R′ is calculated:

$$R' = \varepsilon_{PAR} - (1 - R) = R + \varepsilon_{PAR} - 1 \tag{8.6}$$

In *exp D1* the value of the coefficients used are the ones suggested by Byun et al., (2014) for type III waters.

In *exp D2*, instead of using the generic coefficients for type III waters, new coefficients were estimated by interpolating equation 8.5 over the underwater PAR radiation data provided by the ARPA FVG *in situ* observations. This interpolation was performed using the "curve fitting" tool of the software MATLAB, which is based on a least square method.

EXP E

The *exp E* experiment is based on a new parameterization that derives from a modification of the double exponential parameterization proposed by Byun et al., (2014) (equation8.5) in order to account for phytoplankton self-shading:

$$I(z) = I_0[R'e^{-k_1 z} + (1 - R)e^{-k_2 z}]e^{-k_C \int_0^z P_l(z)dz} \tag{8.7}$$

In this formulation a new exponential term that accounts for the extinction due to chlorophyll-a (P_l) concentration derived

by the Fasham et al., (1983) has been added to the formulation used for *exp D*.

The coefficient used in the implementation of this parameterization in the model are all derived from Byun et al., (2014), except for the chlorophyll attenuation coefficient that had been calculated in Fasham et al., (1983).

The depth varying chlorophyll concentration that determines the phytoplankton self-shading is prognostically calculated by BFM model.

EXP F

The parameterization used in *exp F* is also an original approach. It is similar to equation 8.7 studied in *exp E*, but the term that accounts for the phytoplankton self-shading is now determined by a constant coefficient k_c:

$$I(z) = I_0[R'e^{-k_1 z} + (1 - R)e^{-k_2 z}]e^{-k_c z} \tag{8.8}$$

In the implementation the term k_c has been calculated using the formulation studied by Prieur and Sathyendranath, (1981):

$$k_c = 0.017 + 0.077 * P_l \tag{8.9}$$

Values of k_c were computed for different *in situ* measurements and then averaged over time and depth to obtain the value used in the implementation.

The other coefficients used in equation 8.8 are retrieved by a fit of the underwater PAR values measured by ARPA FVG using the software MATLAB with the same method used for *exp D2*.

9 RESULTS AND DISCUSSION

PAR ATTENUATION PROFILES

The numerical experiments carried out with different algorithms and parameterizations for the PAR underwater penetration in the BFM-POM 1D generated different underwater PAR distributions and consequently different responses of the primary producers (phytoplankton) functional groups.

The simulated PAR profiles at midday have been monthly averaged and have been compared with the observed *in situ* profiles (recorded approximately at the same time). The comparison of the monthly averaged profiles is shown in figure 9.1 that reports the observed PAR profile along with the simulated PAR profiles obtained from each of the numerical experiments described in chapter 8. It can be noted that rather different PAR vertical profiles have been obtained from the different algorithms and parameters.

In figure 9.2 is reported also a more qualitative comparison between the annual cycle of underwater PAR simulated using the different algorithms and parameters and the measured *in situ* data.

To have a quantitative assessment of the performance of the various parameterizations used, the Root Mean Square Error (RMSE) calculated from the simulated and measured PAR data interpolated on the model grid has been calculated. The calculated RMSE profiles are shown in figure 9.3.

In the following figures, the profiles relative to PAR attenuation parameterizations based on a Lambert Beer's single exponential formulation (*exp A*, *exp B1* and *exp B2*) are reported in red; double exponential algorithms based on Byun et al., (2014) are reported in blue (*exp D1* and *exp D2*), while algorithms based on Paulson and Simpson, (1977) with a term that account for phytoplankton self-shading extinction, from Fasham et al., (1983) and Prieur and Sathyendranath, (1981), are reported in

green (*exp C*, *exp E* and *exp F*).

In general, as shown in figures 9.1, 9.2 and 9.3, the parameterizations based on a double exponential formulation (*exp D1*, *exp D2*, *exp C*, *exp E* and *exp F*) provide a better approximation of the PAR attenuation than the ones that derive from a simple Lambert Beer's Law (equation 2.10, implemented in *exp B1* and *exp B2*).

As expected, among the single exponential parameterizations studied, *exp B2*, in which is used a depth-dependent attenuation coefficient $k(z)$ provided by the analysis of the *in situ* PAR measurements from ARPA FVG, approximates better the observed PAR data. The single exponential parameterization studied in *exp B1* is the simplest parameterization for PAR radiation considered and results in the worst estimation of the PAR radiation amount underwater, since it strongly underestimates the attenuation.

The PAR profiles derived from double exponential parameterizations provide a better approximation of the *in situ* observation also with respect to the algorithm implemented by default in the BFM model (*exp A*), which describes the attenuation of radiation with a formulation based on an single exponential with an attenuation coefficient that depends on the contribution to light absorption of different substances such as inorganic suspended matter, particulate detritus and phytoplankton chlorophyll .

The improvement on the simulation of the underwater radiation profiles in the experiments based on a double exponential approach is due to the fact that these parameterizations of PAR attenuation allows a better estimation of the stronger attenuation in the upper part of the water column. In fact, a double exponential function allows the description of the complete absorption of some wavelengths in the first few meters and of the different extinction of the blue-green part of the spectrum, which penetrates more.

It is important to have a good estimation of PAR radiation value in the upper part of the water column especially for the simulation of the primary productivity, that strongly depends on light availability (see chapter 3). A quantitative measure of

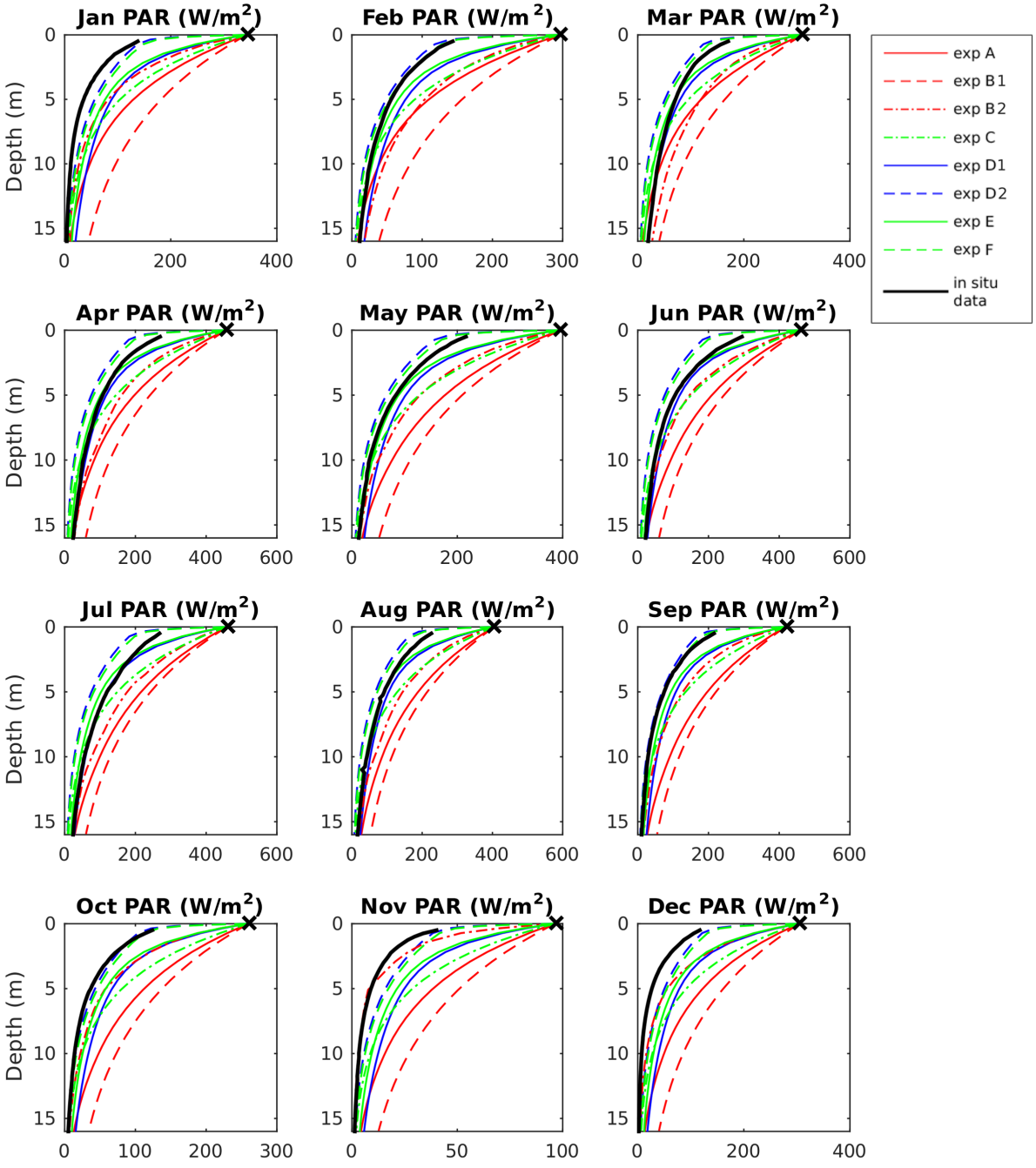

Figure 9.1: Monthly PAR profiles at midday simulated for different parameterizations. **X** represents the value of PAR radiation measured at surface (see chapter 6).

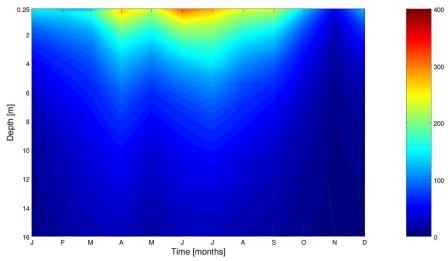

(a)

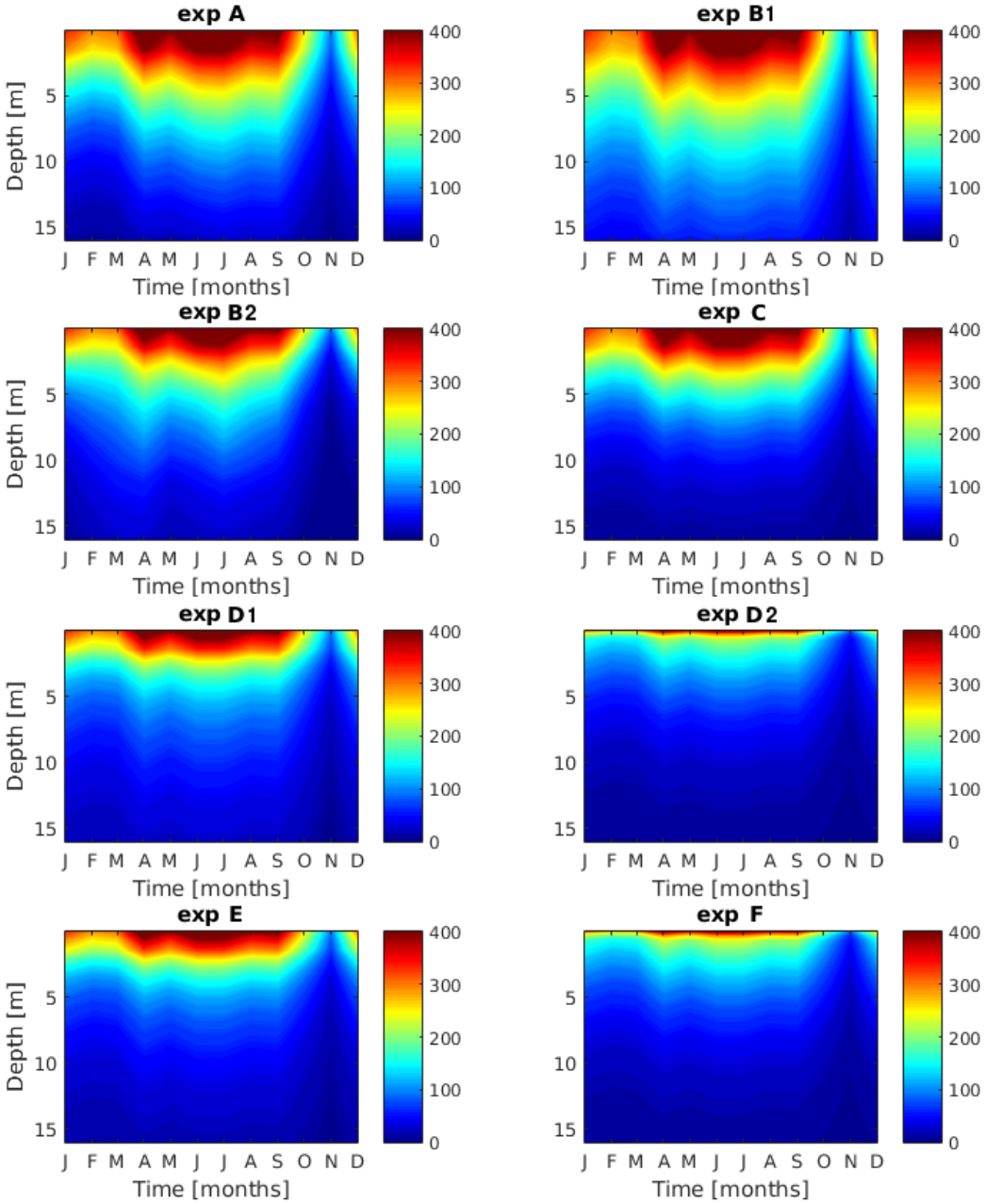

(b)

Figure 9.2: Visualisation of PAR radiation annual cycles simulated with different parameterizations (b) and comparison with the *in situ* data (a). Note that the measured data starts from 0.25 m depth, while the simulated data starts at surface.

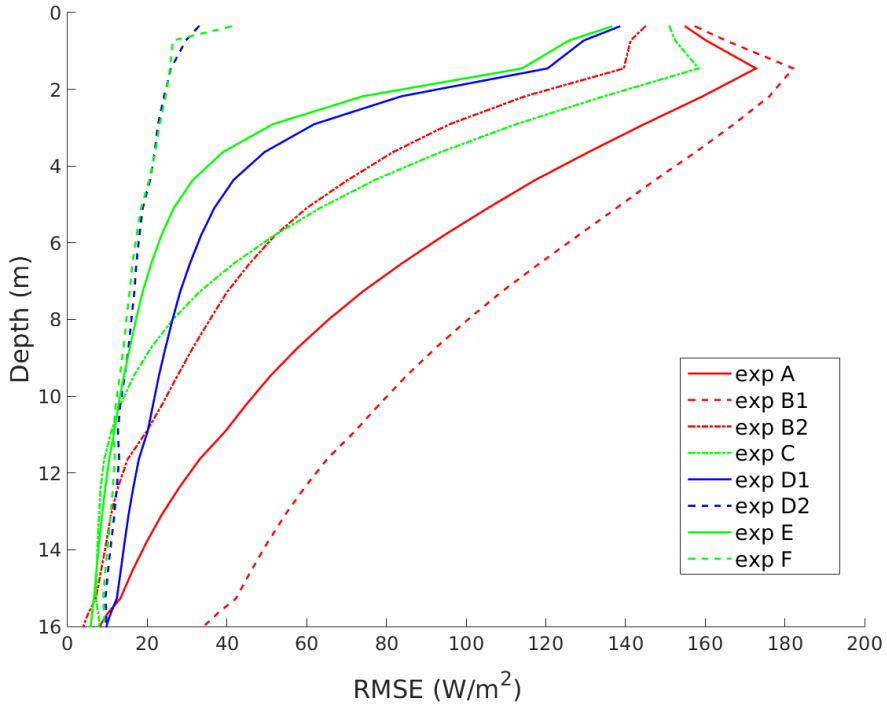

Figure 9.3: RMSE calculated from the simulated and measured PAR data.

the model skill in reproducing observed PAR profiles is given by the RMSE profiles (figure 9.3), computed for all the numerical experiments. The RMSE profiles clearly confirms that double exponential formulations provide a better representation of the measured PAR profiles.

In particular, the improvement of the simulation of the upper water column, where the variability (as shown in figure 9.2) is larger, is seen in *exp D2* and *exp F*. Both of these algorithms use parameters that were estimated from the *in situ* measured data with a procedure described in chapter 8. This allows the algorithms to be adapted to the characteristics of the waters of the Gulf of Trieste.
As we can see in table 8.1, the estimated values of the attenuation coefficient k_1 are considerably greater than the coefficients found in literature and used for the other experiments: this can be seen as a mathematical representation of the strong attenuation observed in the first few centimetres of the water column and accounts for the difference between the amount of incident radiation and radiation immediately below the surface as men-

tioned and discussed in chapter 6.

From the comparison between *exp D1* and *exp E* we can see how adding a term that accounts for the phytoplankton self-shading (*exp E*), depending on the amount of chlorophyll as calculated by the model, improves the estimation of the PAR attenuation.

Improving the simulation of PAR profiles has a significant affect on the performance of the biogeochemical components of the model as shown below.

CHLOROPHYLL ANNUAL CYCLE

The implementation of different parameterization of the PAR attenuation generate different distributions of the underwater PAR, which then constrain the phytoplankton cycle. Figure 9.4 shows the different annual cycles of chlorophyll-a concentration that have been generated from the different PAR parameterizations and in figure 9.5 is shown the Root Mean Square Error calculated between the *in situ* measured Chlorophyll -a profiles and the monthly mean profiles calculated by the BFM-POM 1D model implemented with different PAR attenuation parameterizations.

Figure 9.4 indicates that in general the model underestimates the chlorophyll-a concentration with respect to the observed *in situ* data but there are elements of qualitative agreements between the observations and the simulated values.

In particular the features of the chlorophyll-a annual cycle typical of the gulf of Trieste, such as the autumn bloom and the high concentration of chlorophyll near the bottom during summer, are recognisable in all the simulated cycles.
The simulated cycles that derive from a double exponential parameterization (*exp D1*, *exp D2*, *exp C*, *exp E* and *exp F*) show a stronger chlorophyll-a increase near the seabed in summer and a greater chlorophyll concentration increase towards the sea surface in autumn, which is especially noticeable in *exp D2* and *exp F*.

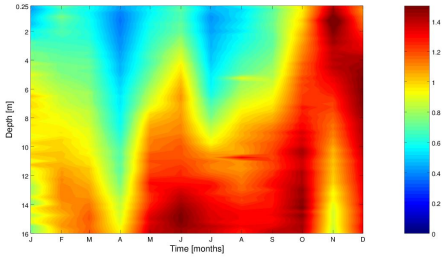

(a)

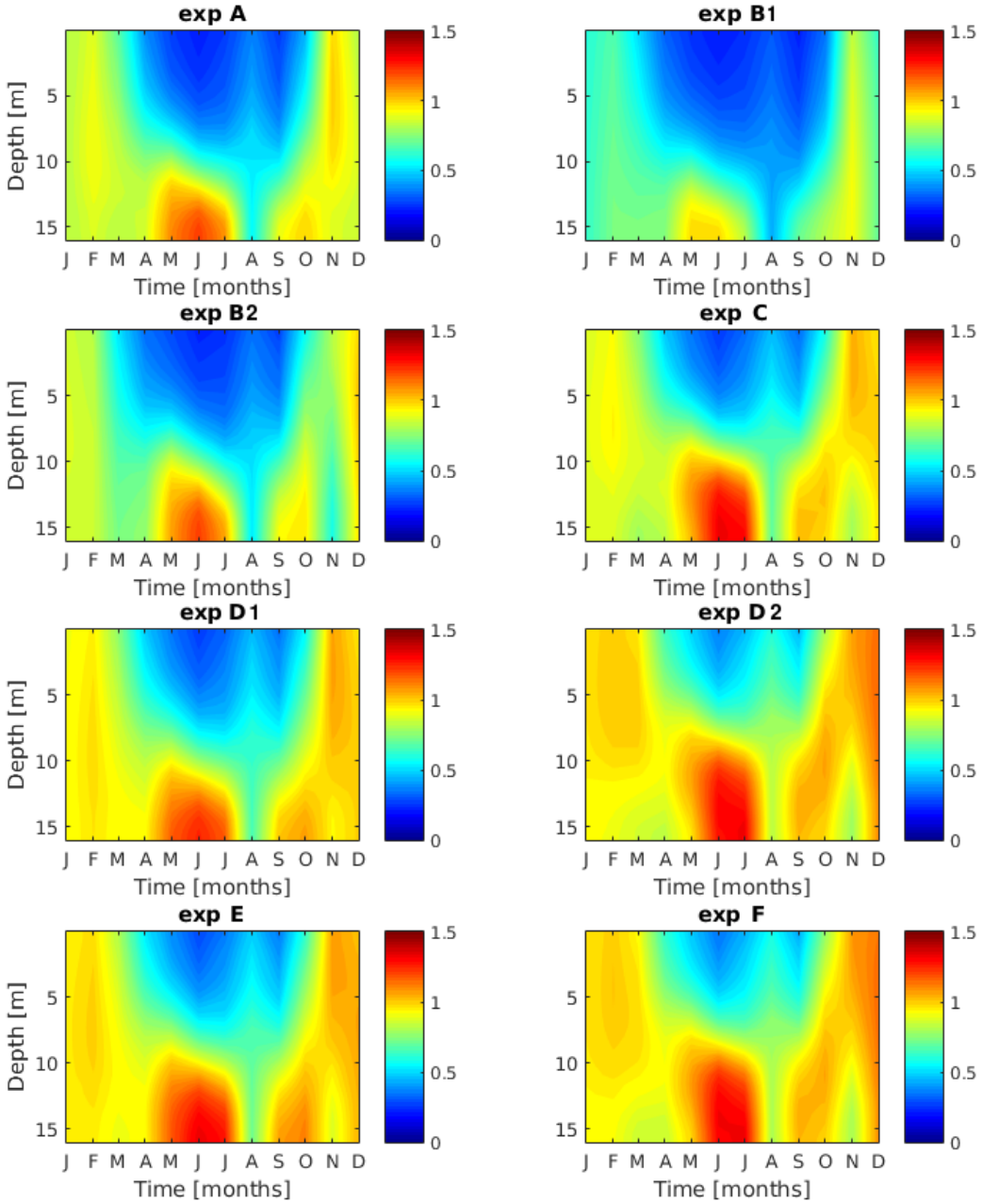

(b)

Figure 9.4: Visualisation of chlorophyll-a annual cycles simulated with different parameterizations (b) and comparison with the *in situ* data (a). Note that the measured data starts from 0.25 m depth, while the simulated data starts at surface.

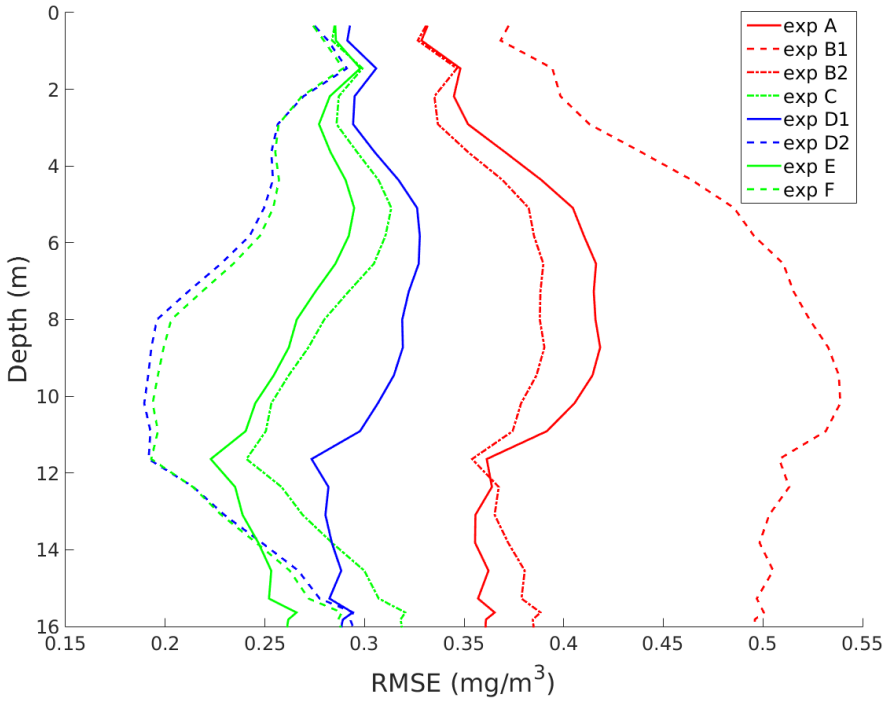

Figure 9.5: RMSE calculated from the simulated and measured chlorophyll-a data.

Some features present in the observed *in situ* data could not be reproduced by the model for all the PAR attenuation algorithms considered. The increase of chlorophyll-a concentration near the seabed in early spring is not reproduced in the simulations, while the subsequent decrease is less intense and the diminution of Chl a in August shown in the simulation near the bottom has no correspondence in the observed data. However, it has to be considered that these differences near the seabed might be due to the benthic-pelagic coupling process description rather than to the light distribution profile.

As we can see in figure 9.5 the parameterizations used in *exp D2* and *exp F* that estimate better the underwater PAR parameterization data measured by ARPA FVG also lead to a better estimation of the Chlorophyll a production compared to the *in situ* measured values, especially in the upper and middle part of the water column. This can be seen also in figure 9.4 as the summer concentrations of chlorophyll-a predicted by *exp D2* and *exp F* are greater in the middle part of the water column compared to the ones predicted by other simulations.

The chlorophyll-a estimation provided by the *exp A*, *exp B2* and especially *exp B1* (figure 9.5) implementation is strongly underestimated in respect to the *in situ* measured data. In figure 9.4 we can see how these experiments do not reproduce some important features of the observed chlorophyll-a cycle. In particular *exp B1* reproduces a great underestimation of the amount of Chl-a during all year and thus has a large associated RMSE.

THE DISSOLVED OXYGEN ANNUAL CYCLE

The dissolved oxygen amount calculated by the model implemented with different PAR parameterization is, in general, overestimated with respect to the *in situ* measured data from ARPA FVG (as shown in figure 9.6). However, the simulated and observed oxygen cycle report similar features: an higher concentration is present in winter due to the water column mixing and consequent ventilation (atmosphere-ocean exchange) and a strong decrease of the amount of dissolved oxygen in summer. The simulated and observed values don't vary much with depth.

The RMSE values (shown in figure 9.7) are larger near the sea surface and decrease with depth for all the algorithms considered in the numerical experiments, meaning that the overestimation of the concentration of dissolved oxygen is stronger in the upper part of the water column and decreases with depth. The largest oxygen RMSE in the upper part of the water column point to an incoherent parameterization of the ocean atmosphere exchanges implemented into BFM according to equation 5.33 based on Wanninkhof, (1992).

In any case the RMSE values arising from the different experiments are characterised by smaller differences among each other. Moreover the better performance of the implementations that describe PAR attenuation utilising a double exponential and the estimated parameter (*exp D2* and *exp F*) is confirmed also from the analysis of the simulated oxygen vertical profiles.

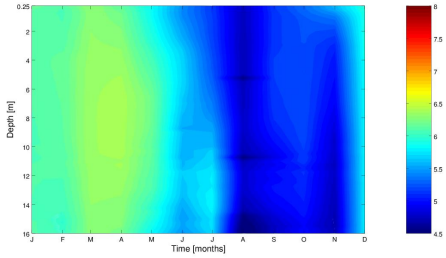

(a)

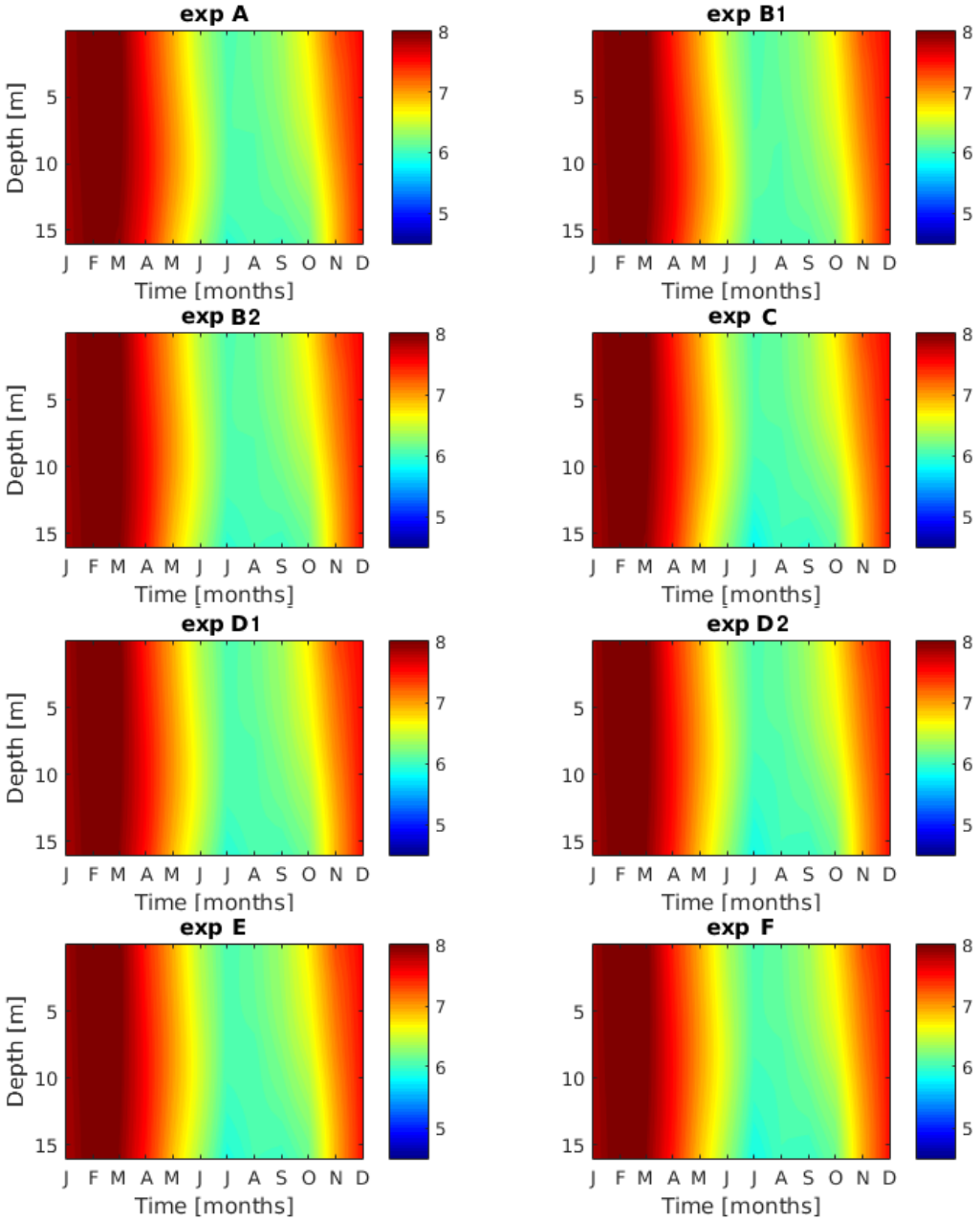

(b)

Figure 9.6: Visualisation of dissolved annual cycles simulated with different parameterizations (b) and comparison with the *in situ* data (a). Note that the measured data starts from 0.25 m depth, while the simulated data starts at surface.

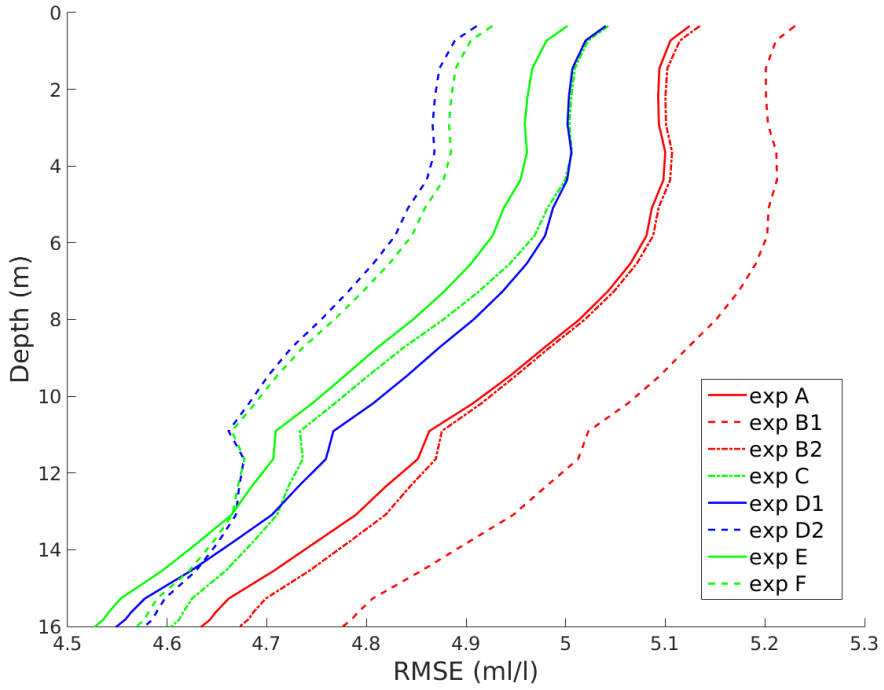

Figure 9.7: RMSE calculated from the simulated and measured dissolved oxygen data.

10

CONCLUSIONS

This study focused on the important issue of the representation of the PAR penetration along the coastal ocean water column in a numerical coupled model (physics and biogeochemistry) that describes the biogeochemical functioning of the marine ecosystem.

The issue has been faced by implementing the BFM-POM 1D numerical system in the Gulf of Trieste, a location for which substantial hydrological, biogeochemical and irradiance data are available and therefore allow for both model validation and development of improvement parameterization of the process.

The systematic implementation of different algorithms and parameterizations, for the definition of the solar radiation penetration along the water column, allowed for a complete evaluation, against *in situ* PAR, chlorophyll and dissolved oxygen data, of the effectiveness of the process description.

As a general finding (and as expected), it turned out that parameterizations based on a double exponential function are able to describe more accurately the PAR underwater rather than classic parameterizations based on a single exponential function. This happens also when the extinction coefficients were computed, as in the default BFM-POM 1D light extinction process description, from the prognostically calculated BFM state variables (chlorophyll-a, particulate organic detritus), available data (suspended sediment concentration) and "ad hoc" conversions factors based on very sparse and scattered (in space and time) direct observations.

In particular, these double exponential functions are able to model the different absorption in the very upper of the water column, due to the rapid absorption of some wavelengths.

The use of a double exponential function to define the PAR vertical distribution in the water column was mutuated from the approach used to define the vertical distribution of the

short wave radiation related heat flux proposed by Paulson and Simpson, (1977). Starting from such contribution, Fasham et al., (1983) included also the phytoplankton self-shading effect, while Byun et al., (2014) improved the definition of the PAR apportioning factor.

The main innovation of this work was the study of specific coefficients based on the analysis of the *in situ* observations provided by ARPA FVG. The parameterizations based on these coefficients proved to be more effective than the ones based on coefficients from literature, especially in the description of the attenuation of the radiation in the first meters of the water column.

Chlorophyll-a concentration and dissolved oxygen concentration calculated by the BFM-POM 1D model, implemented with different algorithms of PAR attenuation, were improved by parameterizations that reproduce better the observed underwater PAR data. In particular, the parameterizations based on the calculated specific coefficients for the Gulf of Trieste allowed the model to simulate more accurately some features of the chlorophyll-a concentration annual cycle like the summer increase near the seabed and the autumn surface bloom.

Conclusively, it has to be remarked that the derived coefficients were based on observations from the coastal ocean: i.e. a location whose characteristics heavily depend not only on the local ecological dynamics but also (and sometimes mostly) on the land-ocean interactions. The obtained parameters for the double exponential algorithm may therefore be affected by the local characteristics of the observed site.
However, the parameters estimated arise from a relative long (2014-2016) observational data set of PAR and chlorophyll-a and might in any case represent an indicative (first guess) parameter set also for different coastal ocean location.

As a final consideration, it has to be stated once more that an adequate observational system working jointly with a modelling system might greatly help to improve the understanding of the coupled coastal marine environmental dynamics.

BIBLIOGRAPHY

Apel, John R. (1987). *Principles of ocean physics*. Vol. 38. Academic Press.

Baker, Edward T. and J. William Lavelle (1984). "The effect of particle size on the light attenuation coefficient of natural suspensions". In: *Journal of Geophysical Research: Oceans* 89.C5, pp. 8197–8203.

Berrisford, P., DK Dee, M. Fuentes, P. Kallberg, S. Kobayashi, and S. Uppala (2009). "The ERA-Interim archive. ERA-40 Report Series No. 1, ECMWF, Shinfield Park". In: *Reading* 10.

Blumberg, Alan F. and George L. Mellor (1987). "A description of a three-dimensional coastal ocean circulation model". In: *Three-dimensional coastal ocean models*, pp. 1–16.

Butenschön, Momme, Marco Zavatarelli, and Marcello Vichi (2012). "Sensitivity of a marine coupled physical biogeochemical model to time resolution, integration scheme and time splitting method". In: *Ocean Modelling* 52, pp. 36–53.

Byun, Do-Seong and Yang-Ki Cho (2006). "Estimation of the PAR irradiance ratio and its variability under clear-sky conditions at Ieodo in the East China Sea". In: *Ocean Science Journal* 41.4, pp. 235–244.

Byun, Do-Seong, Xiao Hua Wang, Deirdre E Hart, and Marco Zavatarelli (2014). "Review of PAR parameterizations in ocean ecosystem models". In: *Estuarine, Coastal and Shelf Science* 151, pp. 318–323.

Fasham, M.J.R., P.M. Holligan, and P.R. Pugh (1983). "The spatial and temporal development of the spring phytoplankton bloom in the Celtic Sea, April 1979". In: *Progress in Oceanography* 12.1, pp. 87–145.

Geider, Richard J., Hugh L. MacIntyre, and Todd M. Kana (1996). "A dynamic model of photoadaptation in phytoplankton". In: *Limnology and Oceanography* 41.1, pp. 1–15.

Hamme, Roberta C. and Steven R. Emerson (2006). "Constraining bubble dynamics and mixing with dissolved gases: Implications for productivity measurements by oxygen mass balance". In: *Journal of Marine Research* 64.1, pp. 73–95.

Jassby, Alan D. and Trevor Platt (1976). "Mathematical formulation of the relationship between photosynthesis and light

for phytoplankton". In: *Limnology and oceanography* 21.4, pp. 540–547.

Jerlov, Nils Gunnar (1976). *Marine optics*. Vol. 14. Elsevier.

Kara, A. Birol, Alan J. Wallcraft, and Harley E. Hurlburt (2005). "A new solar radiation penetration scheme for use in ocean mixed layer studies: an application to the Black Sea using a fine-resolution Hybrid Coordinate Ocean Model (HYCOM)". In: *Journal of physical oceanography* 35.1, pp. 13–32.

Kirk, John TO (1994). *Light and photosynthesis in aquatic ecosystems*. Cambridge university press.

Mussap, Giulia and Marco Zavatarelli (2017). "A numerical study of the benthic–pelagic coupling in a shallow shelf sea (Gulf of Trieste)". In: *Regional Studies in Marine Science* 9, pp. 24–34.

Mussap, Giulia, Marco Zavatarelli, Nadia Pinardi, and Massimo Celio (2016). "A management oriented 1-D ecosystem model: Implementation in the Gulf of Trieste (Adriatic Sea)". In: *Regional Studies in Marine Science* 6, pp. 109–123.

Paulson, Clayton A. and James J. Simpson (1977). "Irradiance measurements in the upper ocean". In: *Journal of Physical Oceanography* 7.6, pp. 952–956.

Payne, Richard E. (1972). "Albedo of the sea surface". In: *Journal of the Atmospheric Sciences* 29.5, pp. 959–970.

Prieur, Louis and Shubha Sathyendranath (1981). "An optical classification of coastal and oceanic waters based on the specific spectral absorption curves of phytoplankton pigments, dissolved organic matter, and other particulate materials." In: *Limnology and Oceanography* 26.4, pp. 671–689.

Sakshaug, Egil, Annick Bricaud, Yves Dandonneau, Paul G. Falkowski, Dale A. Kiefer, Louis Legendre, André Morel, John Parslow, and Masayuki Takahashi (1997). "Parameters of photosynthesis: definitions, theory and interpretation of results". In: *Journal of Plankton Research* 19.11, pp. 1637–1670.

Stravisi, Franco (1998). "Optical seawater properties in the Gulf of Trieste". In: *International Workshop on the "Oceanography of the Adriatic Sea"*. Trieste.

Vichi, Marcello, Nadia Pinardi, and Simona Masina (2007). "A generalized model of pelagic biogeochemistry for the global ocean ecosystem. Part I: Theory". In: *Journal of Marine Systems* 64.1, pp. 89–109.

Wanninkhof, Rik (1992). "Relationship between wind speed and gas exchange over the ocean". In: *Journal of Geophysical Research: Oceans* 97.C5, pp. 7373–7382.